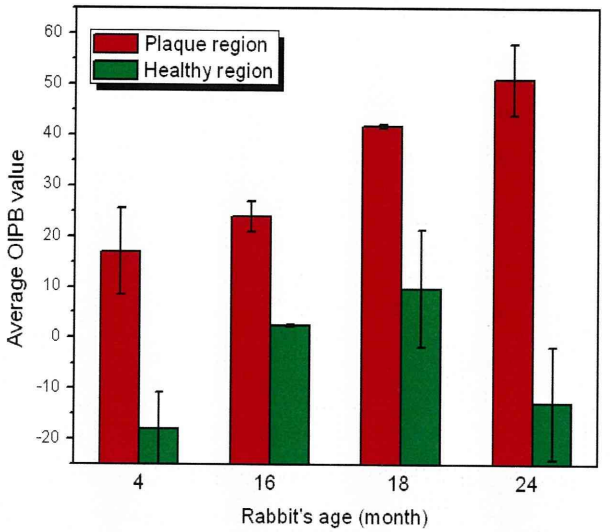

Fig. 7. Mean OIPB indexes of healthy and atherosclerotic lumen surfaces as a function of rabbits' age.

According to previous studies [39,45,46] and the observation in the current study, young WHHLMI rabbits at 4-6 months of age only show lipid streaks on the luminal wall of the aorta while most of the lumen surface remains largely intact. At 15-20 months of age, plaque has accumulated over large areas of the lumen surface of the aorta of the rabbit. Past 20 months, almost the entire rabbit artery is covered with advanced lesions with very limited intact surface. A strong correlation is observed between the OIPB indices and the burden of plaque found in WHHLMI rabbits. Another analysis shows the mean arterial OIPB index for each rabbit pooling all the measurements whether from healthy and plaque dominated regions of the lumen. This age-based mean OIPB index plotted as a function of the age of the rabbit is illustrated in Fig. 8.

So far, we demonstrated that the OIPB index is a better discriminatory parameter compared to the SS scores in differentiating plaque burden. This result also illustrates that inter-channel intensity changes detected among TPEF, SHG and CARS correlate with atherosclerotic plaque progression as evident in Fig. 9 which compares the individual OIPB index of Fig. 5A–5H.

To help visualize the correlation between OIPB index, its corresponding NLO image and the age of the animal, NLO images collected from various healthy areas of lumen and atherosclerotic lesions are shown in Fig. 10 along with the respective OIPB index and rabbit's age.

Figures 10A and 10B show a healthy lumen with a very low OIPB index of −30.8 and -23.6, respectively, and Fig. 10C shows an image with an OIPB of 17.7 taken from an early lesion (or a fatty streak) found in a 4 months-old rabbit artery.

#127944 - $15.00 USD Received 5 May 2010; revised 24 Jun 2010; accepted 25 Jun 2010; published 14 Jul 2010

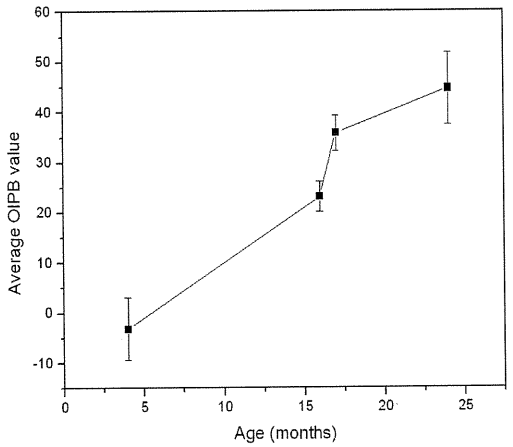

Fig. 8. Mean OIPB indexes of all regions of arterial lumen as a function of rabbits' age.

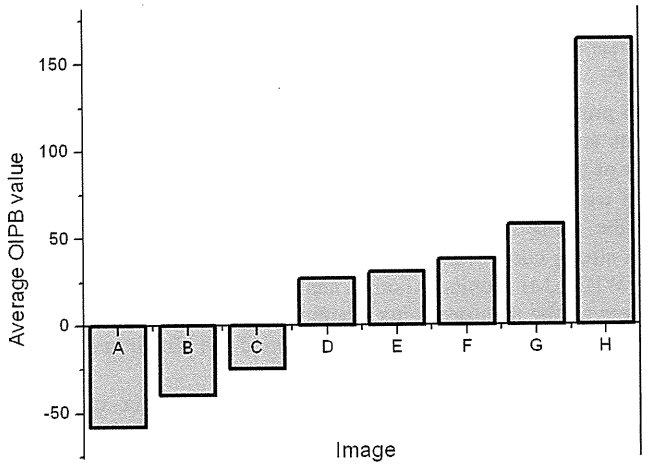

Fig. 9. OIPB indices of all images shown in Fig. 5. OIPB index is a better discriminatory parameter in differentiating plaque burden.

The biochemical tissue morphology looks very different between these three images and this difference is also reflected in their respective OIPB values. Figures 10D and 10E are images of plaques found in the arteries of 16 and 17 months-old rabbits. These lesions are more advanced than that shown in Fig. 10C. The OIPB index for the images in Fig. 10D and 10E are both higher than that of Fig. 10C reflecting the more advanced nature of the plaque. Figure 10F shows an image of the surface of a plaque from a 24 months-old rabbit that died of natural causes. An OIPB index of 109.1 is calculated from this image which is the highest among all those illustrated in Fig. 10.

#127944 - $15.00 USD Received 5 May 2010; revised 24 Jun 2010; accepted 25 Jun 2010; published 14 Jul 2010

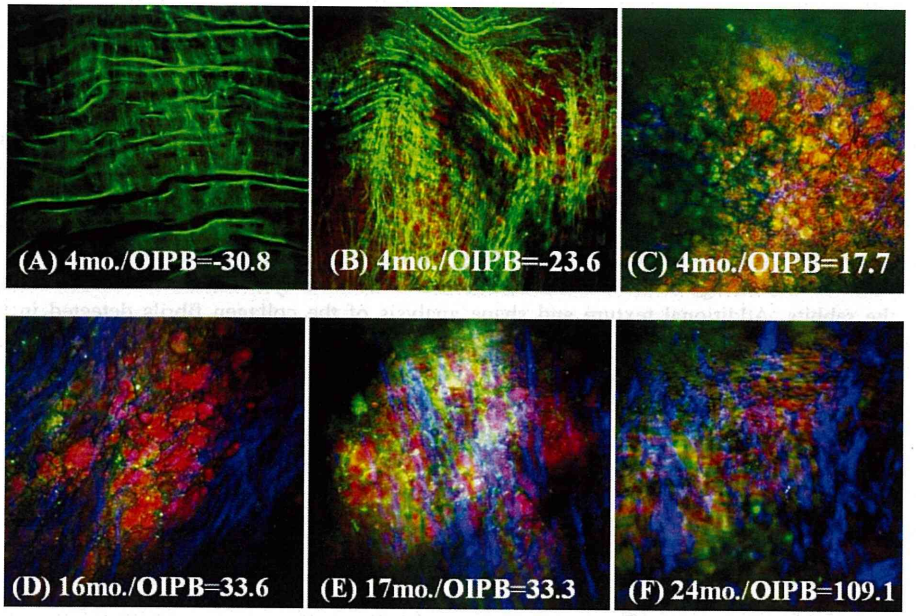

Fig. 10. Representative epi-NLO images obtained from the luminal surface of thoracic aorta of rabbits sacrificed at (A), (B) and (C) 4 months (D) 16 months (E) 17 months and (F) 24 months of age. Images were collected using 20x air objective lens. These are the sum images of 5 consecutive image planes taken at 2 μm steps from 20μm to 30μm beneath the luminal surface. Green is TPEF signal representing elastin fiber and other endogenous fluorescent molecules; Blue is SHG signal representing fibrillar collagen; Red is CARS signal representing lipids-rich structures in plaque.

Correlation analysis using OIPB indices, WHHLMI rabbit age, disease state and biochemical tissue morphology clearly show that younger rabbits with less plaque development have a lower OIPB index with the NLO images of healthy lumen generally having a negative OIPB value. This negative OIPB value is a result of the near-zero significant signal scores, SS_{SHG} and SS_{CARS}, along with the negative values of $d(SS_{SHG}, SS_{TPEF})$ and $d(SS_{CARS}, SS_{TPEF})$ in Eq. (1). As shown in Figs. 3A, 3C, 3E, 3G, 5A, 5B, 5C, 10A and 10B, internal elastic membrane and elastin fibers were often the only major extracellular component in the images of healthy lumen thus resulting in near-zero SS_{SHG} and SS_{CARS} scores. As atherosclerotic lesions progress, either SS_{SHG} (collagen content) or SS_{CARS} (lipids content) or both scores increase, thus leading to higher OIPB values. The last term $d(SS_{CARS}, SS_{SHG})$ in Eq. (1) can help differentiate type $V(V_a)$ from type IV atheroma by distinguishing the relative intensity difference between SHG (mostly from collagen) and CARS (mostly from lipid-rich structures) signals. According to the classification of atherosclerotic lesions provided by American Heart Association [44], type IV lesions are characterized by dense accumulation of extracellular lipid while type V display the formation of prominent new fibrous connective tissue. The $d(SS_{CARS}, SS_{SHG})$ score is therefore more likely to be higher for a type $V(V_a)$ lesion than for a type IV lesion due to higher collagen density this in turn will result in a higher OIPB index for a type $V(V_a)$ atheroma.

Visual investigation of the NLO images not only show the formation of fibrillar collagen and lipid-rich structures on the lumen surface in progressive plaques, but also the texture of the collagen fibrils change during the course of lesion development. For example, an image acquired from an early lesion shows only thin sparse collagen fibrils (Fig. 10C) but in advanced lesions (Fig. 10E and 10F) the collagen fibrils are thicker and more directional. We believe that more detailed texture analysis of fibrillar collagen visualized by SHG could lead

#127944 - $15.00 USD Received 5 May 2010; revised 24 Jun 2010; accepted 25 Jun 2010; published 14 Jul 2010

to further objective measures of plaque development that could augment our current intensity-based model in quantifying plaque burden from label–free NLO imaging of arteries.

4. Conclusion

An intensity-based parameter based on three intrinsic nonlinear optical signals, TPEF, SHG and CARS, collected from images of the lumen surface of the aorta from rabbits was developed that provides a quantitative model for differentiating atherosclerotic plaque burden. This new optical index for plaque burden, OIPB, was defined using the NLO images acquired from ex-vivo samples of un-sectioned bulk rabbit arterial tissue. This index showed a correlation with the age of the WHHLMI rabbits and the severity of the atherosclerotic lesions in the rabbits. Additional texture and shape analysis of the collagen fibrils detected in the SHG imaging of lesions and a larger number of samples could further improve the reliability of the proposed model for the quantification of plaque burden in the WHHLMI model. Given that human plaque development goes through stages of development involving the same key biochemical building blocks that can be sensitively detected by NLO imaging, this work suggests that a similar strategy could be used to develop objective measures to classify human disease based on NLO imaging.

Acknowledgements

We acknowledge Vijay Iyer for his assistance provided in using ScanImage software, Luiz C.B.M. Guidolin for his suggestions in data analysis, and Saro Bascaramurty for performing histological analysis. This work was supported by National Research Council Canada, Genomics and Health Initiative under program "Heart disease: better tools for better treatment".

#127944 - $15.00 USD Received 5 May 2010; revised 24 Jun 2010; accepted 25 Jun 2010; published 14 Jul 2010

ACS Chemical Neuroscience

RESEARCH ARTICLE

pubs.acs.org/acschemicalneuroscience

Rhodanine and Thiohydantoin Derivatives for Detecting Tau Pathology in Alzheimer's Brains

Masahiro Ono,*[,†] Shun Hayashi,[†] Kenji Matsumura,[†] Hiroyuki Kimura,[†] Yoko Okamoto,[‡] Masafumi Ihara,[‡] Ryosuke Takahashi,[‡] Hiroshi Mori,[§] and Hideo Saji*[,†]

[†]Graduate School of Pharmaceutical Sciences, Kyoto University, 46-29 Yoshida Shimoadachi-cho, Sakyo-ku, Kyoto 606-8501, Japan
[‡]Graduate School of Medicine, Kyoto University, 54 Shogoin-kawaharacho, Sakyo-ku, Kyoto 606-8507, Japan
[§]Department of Neuroscience, Osaka City University Medical School, 1-4-3 Asahi-machi, Abeno-ku, Osaka 545-8585, Japan

Supporting Information

ABSTRACT: A novel series of rhodanin (RH) and thiohydantoin (TH) derivatives were designed and synthesized for detecting tau pathology in the brains of patients with Alzheimer's disease (AD). In experiments in vitro using tau and β-amyloid (Aβ) aggregates, the TH derivative, TH2, showed high specific binding to tau aggregates. In hippocampal sections obtained from AD patients, TH2 intensely stained neurofibrillary tangles. In experiments using normal mice, [^{125}I]TH2 showed good uptake (1.54%ID/g, 2 min postinjection) into and a rapid washout (0.25%ID/g, 60 min postinjection) from the brain. [^{123}I]TH2 should be further investigated as a potential imaging agent for detecting tau pathology.

KEYWORDS: Alzheimer's disease, tau, imaging, rhodanine, thiohydantoin

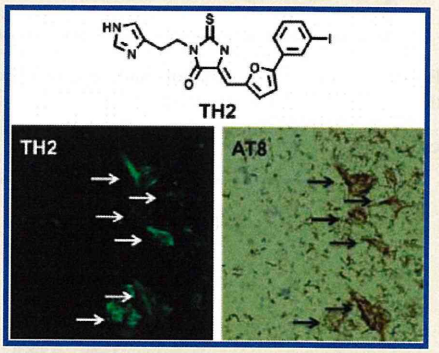

Alzheimer's disease (AD) is a progressive neurodegenerative disorder characterized by abundant senile plaques (SPs) composed of β-amyloid (Aβ) peptides and numerous neurofibrillary tangles (NFTs) formed by filaments of highly phosphorylated tau proteins in the brain.[1] Currently, only the definitive confirmation of AD is dependent on a post-mortem histopathological examination of SPs and NFTs in the brain. Therefore, in vivo imaging of SPs and/or NFTs in the living brain with noninvasive techniques such as positron emission tomography (PET) and single photon emission computed tomography (SPECT) could lead to the presymptomatic detection of AD and new antiamyloid therapies.[2−4]

Extensive research has been undertaken to develop radiolabeled Aβ imaging agents for targeting SPs. Clinical trials with [^{18}F]FDDNP,[5,6] [^{11}C]6-OH-BTA-1,[7,8] [^{11}C]SB-13,[9,10] [^{18}F]BAY94−9172,[11,12] [^{11}C]BF227,[13] [^{123}I]IMPY,[14−17] [^{18}F]AV-45,[18−20] [^{11}C]AZD2184,[21] and [^{18}F]AZD4694[22] indicate the imaging of Aβ plaques in living brain tissue to be useful for the diagnosis of AD.

While many PET/SPECT probes for SPs or Aβ plaques have been developed, few compounds for targeting NFTs have been reported. Previous neuropathological research suggests that the deposition of NFTs occurs before the manifestation of clinical symptoms in AD. These reports suggest that even in the very early stages of AD, patients display considerable numbers of NFTs in the entorhinal cortex and hippocampus, sufficient for a neuropathological diagnosis. Furthermore, NFT deposition in the entorhinal cortex is closely related with neuronal loss in very early AD patients.[23−26] Thus, in vivo imaging of NFTs in conjunction with the imaging of Aβ plaques is thought to be useful for the early and accurate diagnosis of AD. A quantitative evaluation of tau pathology could also be helpful for tracking the severity of dementia, because the pathology correlates well with the clinical severity of dementia.

Some papers have reported that FDDNP,[27] FSB,[28] and curcumin [29] can bind to not only NFTs but also Aβ plaques in the brain. Quinoline and benzimidazole derivatives are also reported as candidate probes for in vivo imaging of tau pathology in AD.[30] However, these compounds are not completely specific to tau, because they also bind to Aβ plaques. Currently, no PET/SPECT imaging agents targeting NFTs exist that allow an evaluation of tau pathology in AD brains.

Recently, the effects of rhodanine and thiohydantoin derivatives on the formation, extension, and destabilization of tau aggregates were studied in vitro.[31] These derivatives dose-dependently inhibited the formation of tau aggregates as well as destabilized preformed tau aggregates, indicating that they could directly bind or interact with the aggregates. In the present study, we designed and synthesized three novel radioiodinated rhodanine and thiohydantoin derivatives (Figure 1) and evaluated their biological activities as in vivo NFT imaging agents. To our knowledge, this is the first time the use of rhodanine and thiohydantoin derivatives in vivo as probes to detect tau pathology in the AD brain has been proposed.

Received: January 17, 2011
Accepted: March 1, 2011
Published: March 21, 2011

RESULTS AND DISCUSSION

Chemistry. The synthesis of the rhodanine and thiohydantoin derivatives was outlined in Scheme 1. The key step in the formation of the rhodanine and thiohydantoin backbone was achieved by a Knoevenagel condensation reaction between aromatic aldehydes and the rhodanine or thiohydantoin core. The aromatic aldehydes (**1** and **8**) necessary for the Knoevenagel condensation reaction were obtained by Suzuki coupling between haloaromatics and functionalized boronic acid. The rhodanin and thiohydantoin cores (**2**, **3**, and **6**) were produced by the reaction of glycine ethyl ester or histamine with bis(carboxymethyl)trithiocarbonate or ethyl isothiocyanotoacetate in the presence of Et_3N. The target compounds (**4** (rhodanin 1 (RH1)), **5** (thiohydantoin 1 (TH1)) and **7** (TH2)) were obtained by the Knoevenagel condensation reaction of the aromatic aldehyde (**1**) with the rhodanin and thiohydantoin cores (**2**, **3**, and **6**) in yields of 76, 44, and 51%, respectively. The tributyltin derivative (**9**) was prepared from the corresponding bromo compound (**8**) using a bromo to tributyltin exchange reaction catalyzed by Pd(**0**) in a yield of 40%. The tributyltin derivatives (**10**, **11**, and **12**) were obtained by the Knoevenagel condensation reaction and used as precursors for radioiodination in the preparation of [^{125}I]RH1, [^{125}I]TH1, and [^{125}I]TH2. Novel radioiodinated rhodanine and thiohydantoin derivatives were obtained with an iododestannylation reaction using hydrogen peroxide as the oxidant, which produced the desired radioiodinated ligands. It was anticipated that the no-carrier-added preparation would result in a final product bearing a theoretical specific activity similar to that of ^{125}I (81.4 TBq/mmol). The radiochemical identities of the radioiodinated ligands were verified by coinjection with nonradioactive compounds from their HPLC profiles. The final radioiodinated compounds [^{125}I]RH1, [^{125}I]TH1, and [^{125}I]TH2 showed a single peak of

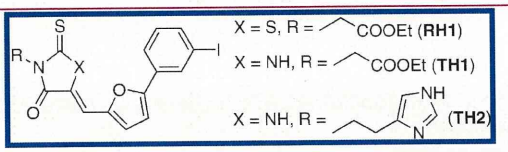

Figure 1. Chemical structure of rhodanine and thiohydantoin derivatives reported in this study.

Scheme 1

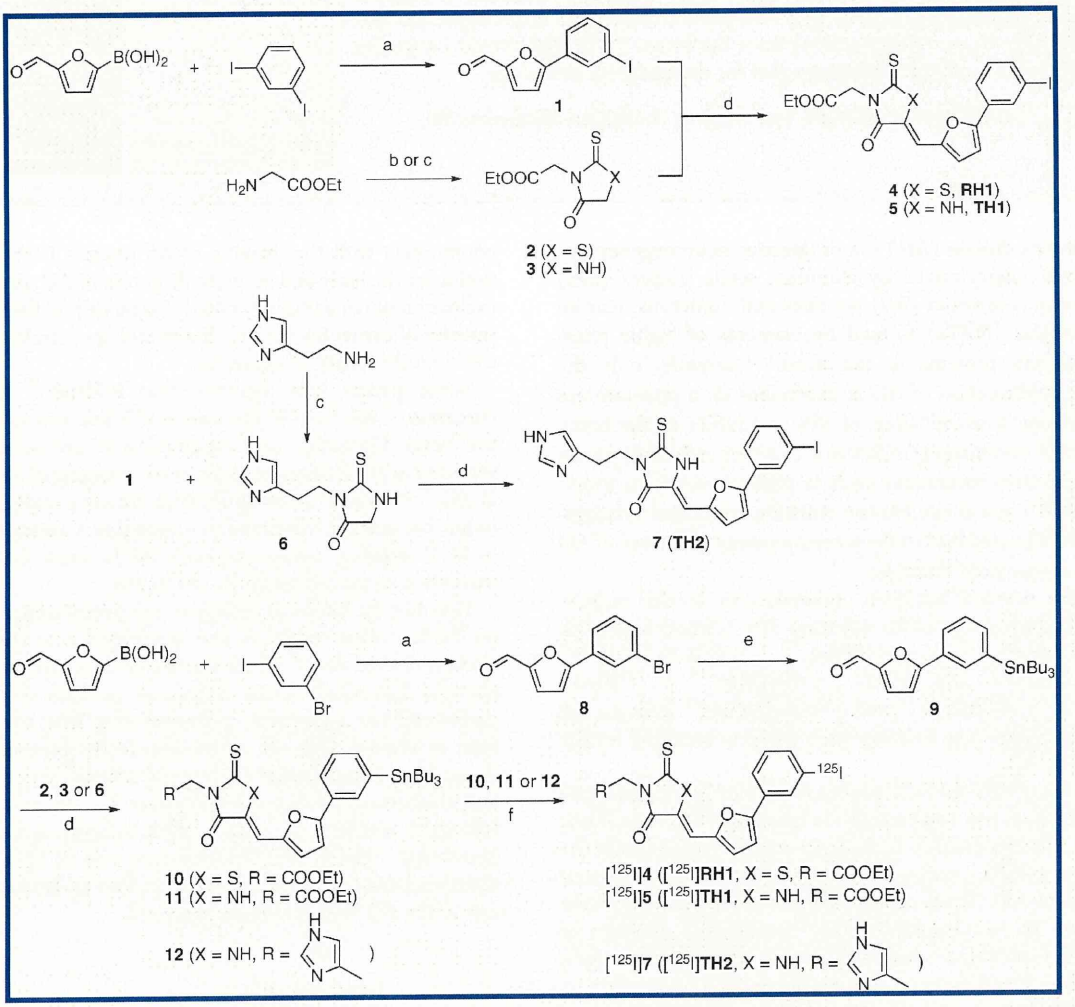

[a] Reagents: (a) $(Ph_3P)_4Pd$, Na_2CO_3, dimethoxyethane. (b) Bis(carboxymethyl)trithiocarnate, Et_3N, *i*PrOH. (c) Ethyl isothiocyanatoacetate, Et_3N, acetonitrile. (d) piperidine, CH_2Cl_2. (e) $(Bu_3Sn)_2$, $(Ph_3P)_4Pd$, Et_3N, dioxane. (f) [^{125}I]NaI, H_2O_2, HCl.

dx.doi.org/10.1021/cn200002t |ACS Chem. Neurosci. 2011, 2, 269–275

Table 1. Inhibition of Thioflavin S Binding to Tau Aggregates or Aβ42 Aggregates

compounds	K_i (nM)[a] tau	Aβ42
RH1	489 ± 62	752 ± 128
TH1	155 ± 14	864 ± 147
TH2	64 ± 7	469 ± 60

[a] Values are the mean ± standard error of the mean for three independent experiments.

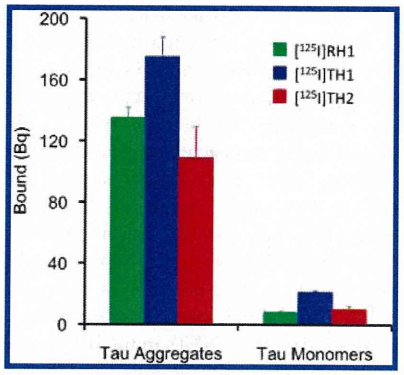

Figure 2. Binding of [^{125}I]RH1, [^{125}I]TH1, and [^{125}I]TH2 to tau aggregates and tau monomers.

radioactivity at the retention times of 9.4 min (CH_3CN/H_2O = 4:1), 15.7 min (CH_3CN/H_2O = 3:2), and 10.5 min (CH_3CN/H_2O = 3:1), respectively. The three products were obtained in 8−22% radiochemical yields with a radiochemical purity of >95% after purification by HPLC.

To quantify the affinity of the rhodanine and thiohydantoin derivatives for tau aggregates, we carried out assays with thioflavin S as a competing ligand. These derivatives displaced thioflavin S in a dose-dependent manner, indicating that they have affinity for tau aggregates. In addition, this result suggests that these derivatives may occupy a binding site on tau aggregates similar to that of thioflavin S. The K_i values for RH1, TH1, and TH2 were 489, 155, and 64 nM, respectively (Table 1). Discrimination between tau and Aβ aggregates in the brain is required for the development of NFT-specific agents. To compare the affinity between tau and Aβ aggregates, we also carried out assays with thioflavin S as a competing ligand. RH1, TH1, and TH2 showed K_i values of 752, 864, and 469 nM, respectively, for Aβ aggregates. The ratio of K_i values for tau and Aβ aggregates was 1.54, 5.57, and 7.33 for RH1, TH1, and TH2, respectively, indicating that these derivatives displayed higher binding to tau aggregates than Aβ aggregates. The result also suggests the thiohydantoin derivatives to be more NFT-selective than the rhodanine derivatives.

Further investigation of the binding to tau aggregates was performed by size exclusion chromatography. A high level of radioactivity was eluted in the fraction corresponding to the tau aggregates after the incubation with [^{125}I]RH1, [^{125}I]TH1, and [^{125}I]TH2 (Figure 2). Conversely, little radioactivity was observed in the fraction corresponding to monomeric tau. The results suggest that these agents bind to tau aggregates not to tau monomers, as reflected by the inhibition assays.

Table 2. Biodistribution of Radioactivity after Intravenous Administration of [^{125}I]RH1, [^{125}I]TH1, and [^{125}I]TH2 in Mice[a]

tissue	time after injection (min) 2	10	30	60
		[^{125}I]RH1		
blood	6.70 (0.53)	3.58 (0.37)	2.27 (0.44)	1.59 (0.14)
liver	43.06 (2.07)	29.52 (2.17)	14.74 (2.27)	11.30 (0.87)
kidney	8.50 (0.83)	7.64 (0.69)	6.42 (1.17)	3.91 (0.18)
intestine	1.77 (0.33)	7.97 (1.24)	15.07 (1.82)	21.03 (2.73)
spleen	6.70 (0.54)	4.11 (0.80)	2.66 (0.84)	1.94 (0.40)
pancreas	1.74 (0.19)	1.75 (0.18)	1.6 (0.17)	0.73 (0.08)
heart	9.41 (0.49)	5.05 (0.39)	2.38 (0.38)	1.39 (0.19)
stomach[b]	0.52 (0.03)	1.16 (0.16)	2.75 (0.36)	2.94 (0.51)
brain	0.23 (0.02)	0.16 (0.01)	0.15 (0.03)	0.11 (0.02)
		[^{125}I]TH1		
blood	9.49 (0.82)	2.38 (0.88)	1.79 (0.11)	1.50 (0.10)
liver	32.19 (1.67)	32.11 (2.09)	22.60 (3.42)	20.18 (1.93)
kidney	9.21 (0.68)	9.311 (1.15)	3.86 (0.85)	2.68 (0.75)
intestine	1.85 (0.26)	7.88 (1.46)	17.73 (2.22)	23.40 (5.37)
spleen	9.16 (2.04)	12.21 (2.28)	13.58 (4.29)	10.04 (2.49)
pancreas	1.79 (0.27)	0.98 (0.08)	0.56 (0.10)	0.45 (0.08)
heart	7.02 (1.23)	2.05 (0.29)	1.19 (0.33)	1.44 (0.39)
stomach[b]	0.62 (0.22)	2.47 (2.41)	2.13 (1.01)	3.30 (1.40)
brain	0.57 (0.0.7)	0.32 (0.02)	0.18(0.02)	0.10 (0.03)
		[^{125}I]TH2		
blood	8.16 (1.21)	2.77 (0.21)	2.11 (0.28)	1.48 (0.27)
liver	34.99 (2.27)	33.32 (1.41)	27.22 (2.05)	22.75 (2.13)
kidney	12.48 (0.76)	7.34 (0.70)	4.97 (0.71)	3.37 (0.30)
intestine	2.55 (0.16)	7.41 (1.21)	17.32 (1.67)	23.58 (2.39)
spleen	9.23 (0.63)	10.87 (2.78)	8.51 (2.68)	8.46 (2.57)
pancreas	3.30 (0.86)	2.15 (0.23)	1.15 (0.18)	0.86 (0.08)
heart	8.48 (0.97)	2.78 (0.19)	1.73 (0.18)	1.30 (0.37)
stomach[b]	0.87 (0.07)	1.70 (1.14)	2.78 (0.68)	5.94 (4.80)
brain	1.54 (0.10)	1.30 (0.12)	0.66 (0.08)	0.25 (0.02)

[a] Expressed as % injected dose per gram. Each value represents the mean (s.d.) for 5 animals at each interval. [b] Expressed as % injected dose per organ.

The biodistribution of the radioiodinated compounds ([^{125}I]RH1, [^{125}I]TH1, and [^{125}I]TH2) was evaluated in normal mice (Table 2). A biodistribution study provides important information on brain uptake. The ideal NFT imaging agent should penetrate the blood−brain barrier well enough to deliver a sufficient dose into the brain while achieving rapid clearance from normal regions to result in a higher signal-to-noise ratio in the AD brain. The initial uptake of [^{125}I]TH2 at 2 min after the iv injection was relatively high (1.54%ID/g), whereas the retention at later time points was low (0.25%ID/g at 60 min post iv injection). These properties (a high initial uptake and fast washout from the normal mouse brain) suggest [^{125}I]TH2 to be a promising NFT imaging agent in the brain. On the other hand, [^{125}I]RH1 and [^{125}I]TH1 did not show marked initial uptake in the brain after iv injection (0.23 and 0.57%ID/g at 2 min postinjection, respectively), though the level of radioactivity in blood was similar to that for [^{125}I]TH2. To directly compare

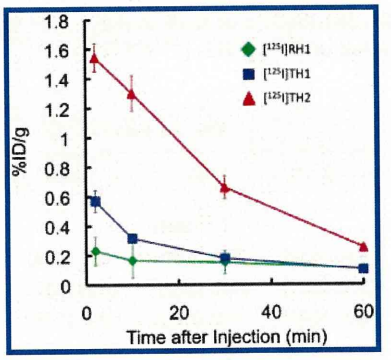

Figure 3. Comparison of brain uptake of [^{125}I]RH1, [^{125}I]TH1, and [^{125}I]TH2 in normal mice.

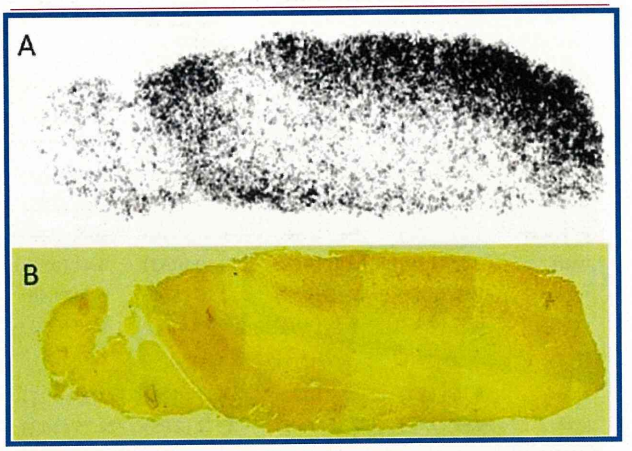

Figure 4. In vitro autoradiograms of sections of AD brain labeled with [^{125}I]TH2 (A). The same sections were immunostained using an antibody against hyperphosphorylated tau (AT8) (B).

the uptake and washout rates of [^{125}I]RH1, [^{125}I]TH1, and [^{125}I]TH2, a combined plot is presented in Figure 3. The pharmacokinetics of [^{125}I]TH2 may provide a better pattern for the distribution of tau in AD brains. Although many factors such as molecular size, ionic charge, and lipophilicity affect the uptake of a compound into the brain, the lower lipophilicity of [^{125}I]TH2 may be one reason for the higher uptake of [^{125}I]TH2. We selected TH2 with high specific binding to tau aggregates and favorable pharmacokinetics in the mouce brain, for additional studies.

Next, the affinity of [^{125}I]TH2 for NFT was investigated using in vitro autroradiography in sections of human AD brain as shown in Figure 4. Autoradiographic images of [^{125}I]TH2 showed high levels of radioactivity in the brain tissue (Figure 4A). Furthermore, we confirmed that the hot spots of [^{125}I]TH2 corresponded with those of in vitro immunohistochemical staining in the same brain sections (Figure 4B).

To further investigate the binding to NFT in AD brain sections, we performed neuropathological fluorescent staining with TH2. Many NFTs were clearly stained with TH2 as reflected in the in vitro assay (Figure 5A). The labeling pattern was consistent with that observed on immunohistochemical labeling with an antibody specific for hyperphosphorylated tau (AT8) (Figure 5B), indicating that TH2 shows specific binding to NFTs. These results demonstrate the feasibility of the use of TH2 as a probe for detecting NFTs in the brains of AD patients.

In conclusion, we successfully designed and synthesized a new series of rhodanine and thiohydantoin derivatives as probes for the in vivo imaging of NFT in the brain. The derivatives, especially TH2, displayed higher affinity for tau aggregates than Aβ aggregates in experiments in vitro. Reflecting the results of the in vitro assays, TH2 clearly stained NFT in AD brain sections. In biodistribution experiments using normal mice, TH2 displayed good penetration of and fast washout from the brain, highly desirable characteristics for in vivo NFT imaging agents. Taken together, the present results suggest that [^{123}I]TH2 should be further investigated as a potential imaging agent for

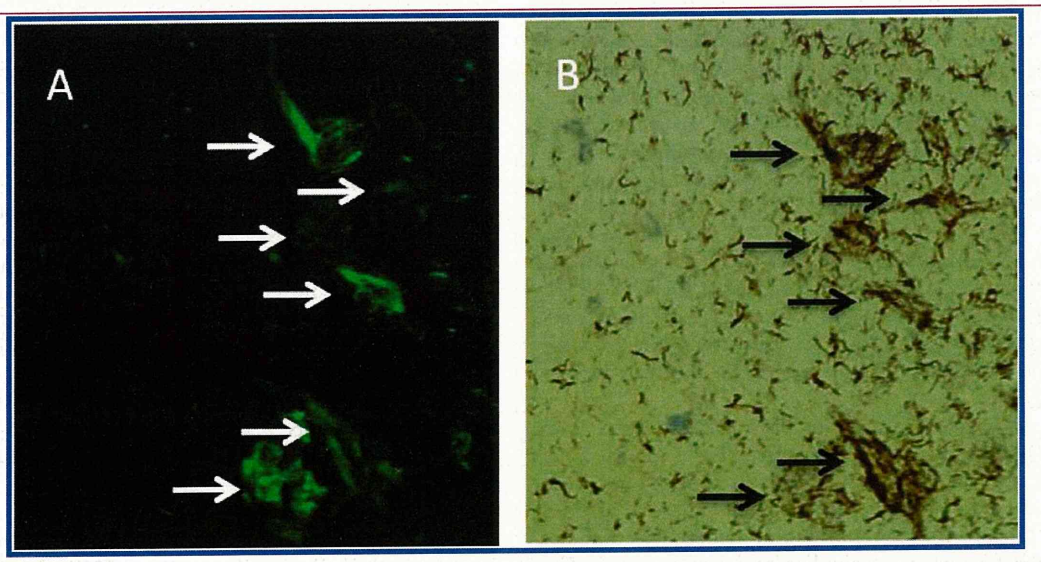

Figure 5. Neuropathological staining of TH2 in 6 μm sections from the hippocampus of an AD patient (A). The same sections were immunostained using an antibody against hyperphosphorylated tau (AT8) (B).

detecting tau pathology. Additional chemical modification of the rhodanine and thiohydantoin structure may lead to more useful NFT imaging agents for both PET and SPECT.

METHODS

General. All reagents were obtained commercially and used without further purification unless otherwise indicated. ^{1}H NMR spectra were obtained on a JEOL JNM400 with TMS as an internal standard. Coupling constants are reported in hertz. Multiplicity was defined by s (singlet), d (doublet), t (triplet), q (quartet), quin (quintet), and m (multiplet). Mass spectra were obtained on a SHIMADZU LCMS-2010 EV. HPLC was performed with a Shimadzu system (a LC-20AT pump with a SPD-10A UV detector, λ = 254 nm) using a Cosmosil C_{18} column (Nakalai Tesque, 5C_{18}-AR-II, 4.6 × 150 mm) and acetonitrile/water (7/3, 3/2, or 3/1) as the mobile phase at a flow rate of 1.0 mL/min. All key compounds were proven by this method to show >95% purity.

Chemistry. *5-(3-Iodophenyl)furan-2-carbaldehyde (**1**).* To a solution of 5-formyl-2-furanboronic acid (280 mg, 2 mmol) and 1,3-diiodobenzene (660 mg, 2 mmol) in dimethoxyethane (15 mL) were added $(Ph_3P)_4Pd$ (114 mg, 0.1 mmol) and 2 M Na_2CO_3 (4.6 mL). The reaction mixture was stirred for 3 h under reflux. Water (20 mL) was added to the cold mixture and extracted with ethyl acetate (20 mL × 2). The organic phase was dried over Na_2SO_4 and filtered. The solvent was removed, and the residue was purified by silica gel chromatography (hexane/ethyl acetate = 7/3) to give 155 mg of **1** (25.9%). ^{1}H NMR (400 MHz, $CDCl_3$) δ 6.85 (d, J = 3.7 Hz, 1H), 7.18 (t, J = 8.0 Hz, 1H), 7.31 (d, J = 3.8 Hz, 1H), 7.74–7.71 (m, 1H), 7.79–7.76 (m, 1H), 8.17 (t, J = 1.7 Hz, 1H), 9.67 (s, 1H).

*Ethyl 2-(4-oxo-2-thioxothiazolidin-3-yl)acetate (**2**).* A mixture of glycine ethyl ester hydrochloride (140 mg, 1 mmol) and bis(carboxymethyl)trithiocarbonate (224 mg, 1 mmol) in a mixed solvent of 2-propanol (6 mL) and triethylamine (0.6 mL) was stirred for 1 h under reflux. The solvent was removed, and the residue was purified by silica gel chromatography (hexane/ethyl acetate = 1/1) to give 177 mg of **2** (80.8%). ^{1}H NMR (400 MHz, $CDCl_3$) δ 1.29 (t, J = 7.2 Hz, 3H), 4.07 (s, 2H), 4.23 (q, J = 7.2 Hz, 2H), 4.72 (s, 2H).

*Ethyl 2-(5-oxo-2-thioxoimidazolidin-1-yl)acetate (**3**).* A mixture of glycine ethyl ester hydrochloride (140 mg, 1 mmol) and ethyl isothiocyanatoacetate (145 mg, 1 mmol) in a mixed solvent of acetonitrile (6 mL) and triethylamine (0.6 mL) was stirred for 10 min at room temperature. The solvent was removed, and the residue was purified by silica gel chromatography (hexane/ethyl acetate = 1/1) to give 170 mg of **3** (84.2%). ^{1}H NMR (400 MHz, $CDCl_3$) δ 1.30 (t, J = 7.2 Hz, 3H), 4.18 (s, 2H), 4.24 (q, J = 7.2 Hz, 2H), 4.57 (s, 2H).

*(Z)-Ethyl 2-(5-((5-(3-iodophenyl)furan-2-yl)methylene)-4-oxo-2-thioxothiazolidin-3-yl) acetate (**4**, RH1).* A mixture of **1** (30 mg, 0.1 mmol) and **2** (22 mg, 0.1 mmol) in dichloromethane (7 mL) and piperidine (20 μL) was stirred for 3 h at room temperature. The solvent was removed, and the residue was purified by silica gel chromatography (hexane/ethyl acetate = 7/3) to give 38 mg of **4** (RH1) (76.2%). ^{1}H NMR (400 MHz, DMSO-d_6) δ 1.21 (t, J = 7.2 Hz, 3H), 4.17 (q, J = 7.2 Hz, 2H), 4.84 (s, 2H), 7.39 (t, J = 8.0 Hz, 1H), 7.43 (d, J = 4.0 Hz, 1H), 7.48 (d, J = 4.0 Hz, 1H), 7.80 (s, 1H), 7.81 (d, J = 8.0 Hz, 1H), 7.88 (d, J = 8.0 Hz, 1H), 8.25 (s, 1H). MS (APCI) m/z 500[MH^+].

*(Z)-Ethyl 2-(4-((5-(3-iodophenyl)furan-2-yl)methylene)-5-oxo-2-thioxoimidazolidin-1-yl) acetate (**5**, TH1).* A mixture of **1** (30 mg, 0.1 mmol) and **3** (20 mg, 0.1 mmol) in dichloromethane (7 mL) and piperidine (20 μL) was stirred for 15 h at room temperature. The residue was removed, and the residue was purified by silica gel chromatography (hexane/ethyl acetate = 7/3) to give 21 mg of **5** (TH1) (43.6%). ^{1}H NMR (400 MHz, DMSO-d_6) δ 1.21 (t, J = 7.2 Hz, 3H), 4.17 (q, J = 7.2 Hz 2H), 4.61 (s, 2H), 6.68 (s, 1H), 7.28 (t, J = 8.0 Hz, 1H), 7.33 (d, J = 4.0 Hz, 1H), 7.38 (d, J = 4.0 Hz, 1H), 7.73 (d, J = 8.0 Hz, 1H), 7.99 (d, J = 8.0 Hz, 1H), 8.34 (s, 1H). MS (APCI) m/z 483[MH^+].

*3-(2-(1H-Imidazol-4-yl)ethyl)-2-thioxoimidazolidin-4-one (**6**).* A mixture of histamine (111 mg, 1 mmol) and ethyl isothiocyanatoacetate (145 mg, 1 mmol) in acetonitrile (6 mL) was stirred for 10 min at room temperature. The solvent was removed, and the residue was purified by silica gel chromatography ($CHCl_3$/MeOH = 4/1) to give 167 mg of **6** (79.5%). ^{1}H NMR (400 MHz, DMSO-d_6) δ 2.77 (t, J = 8.0 Hz, 2H), 3.86 (t, J = 8.0 Hz, 2H), 4.11 (s, 2H), 6.83 (s, 1H), 8.52 (s, 1H), 11.86 (br, s, 1H).

*(Z)-3-(2-(1H-Imidazol-4-yl)ethyl)-5-((5-(3-iodophenyl)furan-2-yl)-methylene)-2-thioxoimidazolidin-4-one (**7**).* A mixture of **1** (30 mg, 0.1 mmol) and **6** (21 mg, 0.1 mmol) in dichloromethane (7 mL) and piperidine (20 μL) was stirred for 3 h at room temperature. The solvent was removed, and the residue was purified by silica gel chromatography (chloroform/MeOH = 9/1) to give 25 mg of **7** (TH2) (51.0%). ^{1}H NMR (400 MHz, DMSO-d_6) δ 2.87 (t, J = 7.6 Hz, 2H), 4.02 (t, J = 7.6 Hz 2H), 6.55 (s, 1H), 6.86 (s, 1H), 7.28 (t, J = 8.0 Hz, 1H), 7.31 (d, J = 4.0 Hz, 1H), 7.35 (d, J = 4.0 Hz, 1H), 7.58 (s, 1H), 7.72 (d, J = 8.0 Hz, 1H), 7.98 (d, J = 8.0 Hz, 1H), 8.32 (s, 1H), 12.14 (br, s, 1H). MS (APCI) m/z 491[MH^+].

*5-(3-Bromophenyl)furan-2-carbaldehyde (**8**).* To a solution of 5-formyl-2-furanboronic acid (676 mg, 4.8 mmol) and 3-bromoiodobenzene (1.13 g, 4 mmol) in dimethoxyethane (30 mL) were added $(Ph_3P)_4Pd$ (228 mg, 0.2 mmol) and 2 M Na_2CO_3 (9.6 mL). The reaction mixture was stirred for 2 h under reflux. Water (20 mL) was added to the cold mixture and extracted with ethyl acetate (20 mL × 2). The combined organic layer was dried over Na_2SO_4 and filtered. The solvent was removed, and the residue was purified by silica gel chromatography (hexane/ethyl acetate = 7/3) to give 306 mg of **8** (25.9%). ^{1}H NMR (400 MHz, $CDCl_3$) δ 6.86 (d, J = 3.7 Hz, 1H), 7.32 (d, J = 3.8 Hz, 1H), 7.34 (t, J = 8.0 Hz, 1H), 7.50–7.53 (m, 1H), 7.73–7.76 (m, 1H), 7.97 (t, J = 1.7 Hz, 1H), 9.68 (s, 1H).

*5-(3-(Tributylstannyl)phenyl)furan-2-carbaldehyde (**9**).* A mixture of **8** (50 mg, 0.2 mmol), bis(tributyltin) (0.4 mL), and $(Ph_3P)_4Pd$ (50 mg, 0.04 mmol) in a mixed solvent (9 mL, 5:4 dioxane/triethylamine mixture) was stirred for 3 h under reflux. The solvent was removed, and the residue was purified by silica gel chromatography (hexane/ethyl acetate = 9/1) to give 37 mg of **9** (40.0%). ^{1}H NMR (400 MHz, $CDCl_3$) δ 0.88–1.66 (m, 27H), 6.83 (d, J = 3.8 Hz, 1H), 7.32 (d, J = 3.8 Hz, 1H), 7.39 (t, J = 8.0 Hz, 1H), 7.48–7.50 (m, 1H), 7.74–7.76 (m, 1H), 7.87 (t, J = 1.2 Hz, 1H), 9.66 (s, 1H).

*(Z)-Ethyl 2-(4-oxo-2-thioxo-5-((5-(3-(tributylstannyl)phenyl)furan-2-yl)methylene)thiazolidin-3-yl)acetate (**10**).* A mixture of **9** (7 mg, 0.015 mmol) and **2** (3.5 mg, 0.016 mmol) in a mixed solvent of dichloromethane (3 mL) and piperidine (5 μL) was stirred for 15 h at room temperature. The solvent was removed, and the residue was purified by silica gel chromatography (hexane/ethyl acetate = 7/3) to give 6 mg of **10** (56.6%). ^{1}H NMR (400 MHz, $CDCl_3$) δ 0.88–1.63 (m, 27H), 1.29 (t, J = 7.0 Hz, 3H), 4.24 (q, J = 7.0 Hz, 2H), 4.87 (s, 2H), 6.87 (d, J = 3.7 Hz, 1H), 6.99 (d, J = 3.7 Hz, 1H), 7.41–7.52 (m, 2H), 7.53 (s, 1H), 7.70–7.73 (m, 2H), 7.91 (s, 1H).

*(Z)-Ethyl 2-(5-oxo-2-thioxo-4-((5-(3-(tributylstannyl)phenyl)furan-2-yl)methylene) imidazolidin-1-yl)acetate (**11**).* To a solution of **9** (10 mg, 0.022 mmol) and **3** (4.4 mg, 0.022 mmol) in dichloromethane (3 mL) was added piperidine (5 μL). The reaction mixture was stirred at room temperature overnight. The solvent was removed, and the residue was purified by silica gel chromatography (hexane/ethyl acetate = 7/3) to give 11 mg of **11** (74.0%). ^{1}H NMR (400 MHz, DMSO-d_6) δ 0.84–1.54 (m, 27H), 1.21 (t, J = 7.6 Hz, 3H), 4.17 (q, J = 7.2 Hz, 2H), 4.60 (s, 2H), 6.67 (s, 1H), 7.22 (d, J = 3.8 Hz, 1H), 7.43–7.45 (m, 3H), 7.88–7.90 (m, 2H). MS (APCI) m/z 645[$M - H^-$].

*(Z)-3-(2-(1H-Imidazol-4-yl)ethyl)-2-thioxo-5-((5-(3-(tributylstannyl)phenyl)furan-2-yl)methylene)imidazolidin-4-one (**12**).* To a solution of **9** (65 mg, 0.14 mmol) and **6** (32 mg, 0.15 mmol) in dichloromethane

(7 mL) was added piperidine (20 μL). The reaction mixture was stirred at room temperature overnight. The solvent was removed, and the residue was purified by silica gel chromatography ($CHCl_3$/MeOH = 9/1) to give 42 mg of **12** (45.9%). ^{1}H NMR (400 MHz, DMSO-d_6) δ 0.84−1.64 (m, 27H), 2.87 (t, J = 7.6 Hz 2H), 4.01 (t, J = 7.6 Hz 2H), 6.55 (s, 1H), 6.84 (s, 1H), 7.20 (d, J = 3.6 Hz, 1H), 7.40−7.44 (m, 3H), 7.54 (s, 1H), 7.86−7.88 (m, 2H), 12.14 (br, s, 1H). MS (APCI) m/z 655[MH^+].

Iododestannylation Reaction. The radioiodinated forms of **4** (RH1), **5** (TH1), and **7** (TH2) were prepared from corresponding tributyltin derivatives by iododestannylation. Briefly, 50 μL of H_2O_2 (3%) was added to a mixture of a tributyltin derivative (100 μg/50 μL in EtOH), [^{125}I]NaI (3.7−7.4 MBq, specific activity 81.4 TBq/mmol), and 100 μL of 1 N HCl in a sealed glass vial. The reaction was allowed to proceed at room temperature for 5 min and terminated by the addition of 100 μL of saturated aqueous $NaHSO_3$. After addition of 100 μL of a saturated aqueous $NaHCO_3$, the reaction was extracted with ethyl acetate (1 mL). The extract was dried by passing through an anhydrous Na_2SO_4 column and then blown dry with a stream of nitrogen gas. The radioiodinated ligands were purified by HPLC on a Cosmosil C_{18} column with an isocratic solvent of H_2O/acetonitrile (3/7, 2/3, or 1/3 for RH1, TH, or TH2, respectively) at a flow rate of 1.0 mL/min.

Binding Experiments Using Recombinant Tau and Aβ(1−42) Aggregates. The 441 aa isoform of human tau was expressed from a cDNA clone in *Escherichia coli* and purified as described previously.[32] Tau aggregates were prepared by incubating tau protein (1 mg/mL) in the presence of heparin (0.1 mg/mL) for 72 h with continuous shaking.[30] A solid form of Aβ(1−42) was purchased from Peptide Institute (Osaka, Japan). Aggregation was carried out by gently dissolving the peptide (0.25 mg/mL) in a buffer solution (pH 7.4) containing 10 mM sodium phosphate and 1 mM EDTA. The solution was incubated at 37 °C for 42 h with gentle and constant shaking.

Thioflavin S was used as the tracer for the competition binding experiments. A mixture (100 μL of 10% EtOH) containing RH1, TH1, and TH2 (final conc. 0−10 μM), thioflavin S (final conc. 1.5 μM), and tau aggregates (final conc. 0.2 μM) or Aβ(1−42) aggregates (final conc. 2.2 μM) was incubated at room temperature for 30 min. Fluorescence intensity at an excitation wavelength of 510 nm for tau and 490 nm for Aβ(1−42), respectively, was plotted, and values for the half-maximal inhibitory concentration (IC_{50}) were determined from displacement curves of three independent experiments using GraphPad Prism software (GraphPad Software, San Diego, CA). The inhibition constants (K_i) were calculated using the Cheng-Prusoff equation:[33] $K_i = IC_{50}/(1 + [L]/K_d)$, where $[L]$ is the concentration of thioflavin S used in the assay and K_d is the dissociation constant of thioflavin S. The K_d value for tau and Aβ aggregates was 0.63 and 2.2 μM, respectively. (See Supporting Information.)

Binding Experiments Using Tau Monomers and Tau Aggregates. Tau aggregates were prepared as described above, and the tau monomer was used without aggregation. A mixture (300 μL of 10% EtOH) containing [^{125}I]RH1, [^{125}I]TH1, and [^{125}I]TH2 (2.03 kBq) and the monomer or aggregates (final conc. 0.37 μM) were incubated at room temperature for 10 min. The reaction mixture was fractionated by size exclusion chromatography (PD-10 column, GE Healthcare) using phosphate-buffered saline (PBS) as the mobile phase, and the fraction in which tau aggregates or tau monomers were eluted was obtained. The radioactivity in this fraction was measured with a gamma counter (Perkin-Elmer, WIZARD 1470).

Biodistribution in Normal Mice. The experiments with animals were conducted in accordance with our institutional guidelines and approved by the Kyoto University Animal Care Committee. A saline solution (100 μL) of ^{125}I-labeled derivatives (7.1−21.5 kBq) containing ethanol (10 μL) was injected intravenously directly into the tail of ddY mice (5 weeks old, 22−25 g). The mice were sacrificed at various time points postinjection. The organs of interest were removed and weighed, and radioactivity was measured with an automatic gamma counter (Perkin-Elmer, WIZARD^3 1480).

Neuropathological Staining of AD Brain Sections. Postmortem brain tissues from an autopsy-confirmed case of an AD (93-year-old female) patient were obtained and examined neuropathologically by conventional silver staining. Experiments were performed according to the regulations of the ethics committee of Kyoto University. Six-micrometer-thick serial sections of paraffin-embedded blocks of the hippocampus were used for staining. Paraffin sections were subjected to two 5 min incubations in xylene, and two 1 min incubations in 100% EtOH to completely deparaffinize them, followed by two 5 min washes in water and then PBS. Tissue sections were immersed in the compound solution (200 μM) containing 50% ethanol for 1 h. Finally, the sections were washed in 50% ethanol for 10 min. Fluorescent sections were viewed using a BZ-9000 fluoromicroscope equipped with a GFP-B filter. The sections were also immunostained with DAB as a chromogen using monoclonal antibodies against hyperphosphorylated tau (AT8)[30] as described previously.

In Vitro Autoradiography. Postmortem brain tissues from an autopsy-confirmed case of AD (72-year-old male) were obtained from BioChain Institute Inc. The presence and distribution of NFT in the sections were confirmed with immunohistochemical staining using a monoclonal tau antibody, AT8 (Wako), as reported. The sections were incubated with [^{125}I]TH2 (3.05 kBq/ml) for 1 h at room temperature. They were then dipped in saturated lithium carbonate in 50% EtOH (two 2 min washes) and washed with 50% EtOH (one 2 min wash), before being rinsed with water for 30 s. After drying, the ^{125}I-labeled sections were exposed to a Fuji Film imaging plate overnight.

■ ASSOCIATED CONTENT

Supporting Information. Method for saturation assay with thioflavin S using recombinant tau and $Aβ_{1-42}$ aggregates; figure of binding of thioflavin S to tau aggregates and Aβ aggregates. This material is available free of charge via the Internet at http://pubs.acs.org.

■ AUTHOR INFORMATION

Corresponding Author

*M.O.: phone, +81-75-753-4608; fax, +81-75-753-4568; e-mail, ono@pharm.kyoto-u.ac.jp. H.S.: phone, +81-75-753-4556; fax, +81-75-753-4568; e-mail, hsaji@pharm.kyoto-u.ac.jp.

Author Contributions

M.O. and H.S. oversaw and designed all experiments. S.H. performed synthetic chemistry work, and *in vitro* and *in vivo* experiments. K.M. performed biodistribution studies in normal mice. H.K. oversaw and performed synthetic chemistry work. Y.O., M.I. and R.T. oversaw and performed neuropathological staining of Alzheimer's brain sections. H.M. oversaw and designed binding experiments using tau protein.

Funding Sources

This study was supported by the Funding Program for Next Generation World-Leading Researchers and a Grant-in-aid for Young Scientists (A) and Exploratory Research from the Ministry of Education, Culture, Sports, Science, and Technology, Japan.

■ REFERENCES

(1) Selkoe, D. J. (2001) Alzheimer's disease: genes, proteins, and therapy. *Physiol. Rev. 81*, 741−766.

(2) Mathis, C. A., Wang, Y., and Klunk, W. E. (2004) Imaging β-amyloid plaques and neurofibrillary tangles in the aging human brain. *Curr. Pharm. Des. 10*, 1469–1492.

(3) Nordberg, A. (2004) PET imaging of amyloid in Alzheimer's disease. *Lancet Neurol. 3*, 519–527.

(4) Ono, M. (2009) Development of positron-emission tomography/single-photon emission computed tomography imaging probes for *in vivo* detection of β-amyloid plaques in Alzheimer's brains. *Chem. Pharm. Bull. (Tokyo) 57*, 1029–1039.

(5) Agdeppa, E. D., Kepe, V., Liu, J., Flores-Torres, S., Satyamurthy, N., Petric, A., Cole, G. M., Small, G. W., Huang, S. C., and Barrio, J. R. (2001) Binding characteristics of radiofluorinated 6-dialkylamino-2-naphthylethylidene derivatives as positron emission tomography imaging probes for β-amyloid plaques in Alzheimer's disease. *J. Neurosci. 21*, RC189.

(6) Shoghi-Jadid, K., Small, G. W., Agdeppa, E. D., Kepe, V., Ercoli, L. M., Siddarth, P., Read, S., Satyamurthy, N., Petric, A., Huang, S. C., and Barrio, J. R. (2002) Localization of neurofibrillary tangles and β-amyloid plaques in the brains of living patients with Alzheimer disease. *Am. J. Geriatr. Psychiatry 10*, 24–35.

(7) Mathis, C. A., Wang, Y., Holt, D. P., Huang, G. F., Debnath, M. L., and Klunk, W. E. (2003) Synthesis and evaluation of ^{11}C-labeled 6-substituted 2-arylbenzothiazoles as amyloid imaging agents. *J. Med. Chem. 46*, 2740–2754.

(8) Klunk, W. E., Engler, H., Nordberg, A., Wang, Y., Blomqvist, G., Holt, D. P., Bergstrom, M., Savitcheva, I., Huang, G. F., Estrada, S., Ausen, B., Debnath, M. L., Barletta, J., Price, J. C., Sandell, J., Lopresti, B. J., Wall, A., Koivisto, P., Antoni, G., Mathis, C. A., and Langstrom, B. (2004) Imaging brain amyloid in Alzheimer's disease with Pittsburgh Compound-B. *Ann. Neurol. 55*, 306–319.

(9) Ono, M., Wilson, A., Nobrega, J., Westaway, D., Verhoeff, P., Zhuang, Z. P., Kung, M. P., and Kung, H. F. (2003) ^{11}C-labeled stilbene derivatives as Aβ-aggregate-specific PET imaging agents for Alzheimer's disease. *Nucl. Med. Biol. 30*, 565–571.

(10) Verhoeff, N. P., Wilson, A. A., Takeshita, S., Trop, L., Hussey, D., Singh, K., Kung, H. F., Kung, M. P., and Houle, S. (2004) In-vivo imaging of Alzheimer disease β-amyloid with [^{11}C]SB-13 PET. *Am. J. Geriatr. Psychiatry 12*, 584–595.

(11) Zhang, W., Oya, S., Kung, M. P., Hou, C., Maier, D. L., and Kung, H. F. (2005) F-18 polyethyleneglycol stilbenes as PET imaging agents targeting Aβ aggregates in the brain. *Nucl. Med. Biol. 32*, 799–809.

(12) Rowe, C. C., Ackerman, U., Browne, W., Mulligan, R., Pike, K. L., O'Keefe, G., Tochon-Danguy, H., Chan, G., Berlangieri, S. U., Jones, G., Dickinson-Rowe, K. L., Kung, H. P., Zhang, W., Kung, M. P., Skovronsky, D., Dyrks, T., Holl, G., Krause, S., Friebe, M., Lehman, L., Lindemann, S., Dinkelborg, L. M., Masters, C. L., and Villemagne, V. L. (2008) Imaging of amyloid β in Alzheimer's disease with ^{18}F-BAY94-9172, a novel PET tracer: proof of mechanism. *Lancet Neurol. 7*, 129–135.

(13) Kudo, Y., Okamura, N., Furumoto, S., Tashiro, M., Furukawa, K., Maruyama, M., Itoh, M., Iwata, R., Yanai, K., and Arai, H. (2007) 2-(2-[2-Dimethylaminothiazol-5-yl]ethenyl)-6-(2-[fluoro]ethoxy)benzoxazole: a novel PET agent for *in vivo* detection of dense amyloid plaques in Alzheimer's disease patients. *J. Nucl. Med. 48*, 553–561.

(14) Kung, M. P., Hou, C., Zhuang, Z. P., Zhang, B., Skovronsky, D., Trojanowski, J. Q., Lee, V. M., and Kung, H. F. (2002) IMPY: an improved thioflavin-T derivative for *in vivo* labeling of β-amyloid plaques. *Brain Res. 956*, 202–210.

(15) Zhuang, Z. P., Kung, M. P., Wilson, A., Lee, C. W., Plossl, K., Hou, C., Holtzman, D. M., and Kung, H. F. (2003) Structure-activity relationship of imidazo[1,2-a]pyridines as ligands for detecting β-amyloid plaques in the brain. *J. Med. Chem. 46*, 237–243.

(16) Kung, M. P., Hou, C., Zhuang, Z. P., Cross, A. J., Maier, D. L., and Kung, H. F. (2004) Characterization of IMPY as a potential imaging agent for β-amyloid plaques in double transgenic PSAPP mice. *Eur. J. Nucl. Med. Mol. Imaging 31*, 1136–1145.

(17) Newberg, A. B., Wintering, N. A., Clark, C. M., Plossl, K., Skovronsky, D., Seibyl, J. P., Kung, M. P., and Kung, H. F. (2006) Use of ^{123}I IMPY SPECT to differentiate Alzheimer's disease from controls. *J. Nucl. Med. 47*, 78P.

(18) Zhang, W., Kung, M. P., Oya, S., Hou, C., and Kung, H. F. (2007) ^{18}F-labeled styrylpyridines as PET agents for amyloid plaque imaging. *Nucl. Med. Biol. 34*, 89–97.

(19) Choi, S. R., Golding, G., Zhuang, Z., Zhang, W., Lim, N., Hefti, F., Benedum, T. E., Kilbourn, M. R., Skovronsky, D., and Kung, H. F. (2009) Preclinical properties of ^{18}F-AV-45: a PET agent for Aβ plaques in the brain. *J. Nucl. Med. 50*, 1887–1894.

(20) Kung, H. F., Choi, S. R., Qu, W., Zhang, W., and Skovronsky, D. (2010) ^{18}F stilbenes and styrylpyridines for PET imaging of Aβ plaques in Alzheimer's disease: a miniperspective. *J. Med. Chem. 53*, 933–941.

(21) Johnson, A. E., Jeppsson, F., Sandell, J., Wensbo, D., Neelissen, J. A., Jureus, A., Strom, P., Norman, H., Farde, L., and Svensson, S. P. (2009) AZD2184: a radioligand for sensitive detection of β-amyloid deposits. *J. Neurochem. 108*, 1177–1186.

(22) Jureus, A., Swahn, B. M., Sandell, J., Jeppsson, F., Johnson, A. E., Johnstrom, P., Neelissen, J. A., Sunnemark, D., Farde, L., and Svensson, S. P. (2010) Characterization of AZD4694, a novel fluorinated Aβ plaque neuroimaging PET radioligand. *J. Neurochem. 114*, 784–794.

(23) Arriagada, P. V., Growdon, J. H., Hedley-Whyte, E. T., and Hyman, B. T. (1992) Neurofibrillary tangles but not senile plaques parallel duration and severity of Alzheimer's disease. *Neurology 42*, 631–639.

(24) Braak, H., and Braak, E. (1993) Entorhinal-hippocampal interaction in mnestic disorders. *Hippocampus 3 Spec. No.* 239–246.

(25) Gomez-Isla, T., Hollister, R., West, H., Mui, S., Growdon, J. H., Petersen, R. C., Parisi, J. E., and Hyman, B. T. (1997) Neuronal loss correlates with but exceeds neurofibrillary tangles in Alzheimer's disease. *Ann. Neurol. 41*, 17–24.

(26) Gomez-Isla, T., Wasco, W., Pettingell, W. P., Gurubhagavatula, S., Schmidt, S. D., Jondro, P. D., McNamara, M., Rodes, L. A., DiBlasi, T., Growdon, W. B., Seubert, P., Schenk, D., Growdon, J. H., Hyman, B. T., and Tanzi, R. E. (1997) A novel presenilin-1 mutation: increased β-amyloid and neurofibrillary changes. *Ann. Neurol. 41*, 809–813.

(27) Small, G. W., Kepe, V., Ercoli, L. M., Siddarth, P., Bookheimer, S. Y., Miller, K. J., Lavretsky, H., Burggren, A. C., Cole, G. M., Vinters, H. V., Thompson, P. M., Huang, S. C., Satyamurthy, N., Phelps, M. E., and Barrio, J. R. (2006) PET of brain amyloid and tau in mild cognitive impairment. *N. Engl. J. Med. 355*, 2652–2663.

(28) Velasco, A., Fraser, G., Delobel, P., Ghetti, B., Lavenir, I., and Goedert, M. (2008) Detection of filamentous tau inclusions by the fluorescent Congo red derivative FSB [(trans,trans)-1-fluoro-2,5-bis(3-hydroxycarbonyl-4-hydroxy)styrylbenzene]. *FEBS Lett. 582*, 901–906.

(29) Mohorko, N., Repovs, G., Popovic, M., Kovacs, G. G., and Bresjanac, M. (2010) Curcumin labeling of neuronal fibrillar tau inclusions in human brain samples. *J. Neuropathol. Exp. Neurol. 69*, 405–414.

(30) Okamura, N., Suemoto, T., Furumoto, S., Suzuki, M., Shimadzu, H., Akatsu, H., Yamamoto, T., Fujiwara, H., Nemoto, M., Maruyama, M., Arai, H., Yanai, K., Sawada, T., and Kudo, Y. (2005) Quinoline and benzimidazole derivatives: candidate probes for *in vivo* imaging of tau pathology in Alzheimer's disease. *J. Neurosci. 25*, 10857–10862.

(31) Bulic, B., Pickhardt, M., Khlistunova, I., Biernat, J., Mandelkow, E. M., Mandelkow, E., and Waldmann, H. (2007) Rhodanine-based tau aggregation inhibitors in cell models of tauopathy. *Angew. Chem., Int. Ed. Engl. 46*, 9215–9219.

(32) Han, D., Qureshi, H. Y., Lu, Y., and Paudel, H. K. (2009) Familial FTDP-17 missense mutations inhibit microtubule assembly-promoting activity of tau by increasing phosphorylation at Ser202 in vitro. *J. Biol. Chem. 284*, 13422–13433.

(33) Cheng, Y., and Prusoff, W. (1973) Relationship between the inhibition constant (K1) and the concentration of inhibitor which causes 50% inhibition (I50) of an enzymatic reaction. *Biochem. Pharmacol. 22*, 3099–3108.

View Online / Journal Homepage / Table of Contents for this issue
Dynamic Article Links

MedChemComm

Cite this: *Med. Chem. Commun.*, 2011, **2**, 596

www.rsc.org/medchemcomm

CONCISE ARTICLE

Phenyldiazenyl benzothiazole derivatives as probes for *in vivo* imaging of neurofibrillary tangles in Alzheimer's disease brains†

Kenji Matsumura,[a] Masahiro Ono,*[a] Shun Hayashi,[a] Hiroyuki Kimura,[a] Yoko Okamoto,[b] Masafumi Ihara,[b] Ryosuke Takahashi,[b] Hiroshi Mori[c] and Hideo Saji*[a]

Received 4th February 2011, Accepted 17th March 2011
DOI: 10.1039/c1md00034a

This paper describes the synthesis and biological evaluation of novel phenyldiazenyl benzothiazole (PDB) derivatives as probes for imaging neurofibrillary tangles (NFTs) in patients with Alzheimer's disease (AD). We successfully synthesized three PDB derivatives using a diazo coupling reaction. In binding experiments *in vitro*, the compounds displayed higher affinity for tau aggregates than for Aβ aggregates. In fluorescent staining experiments using AD brain sections, **9** visualized NFTs clearly. No-carrier-added radioiodinated PDB derivatives were successfully prepared through an iododestannylation reaction from the corresponding tributyltin derivatives. [^{125}I]**9** labeled NFTs in sections of brain tissue from a patient with AD, but not a control. In biodistribution experiments using normal mice, the PDB derivatives displayed an uptake into the brain, sufficient for imaging NFTs, ranging from 0.94 to 3.2% ID g^{-1}, but a relatively slow washout. Although further modifications are necessary to improve the pharmacokinetics in the brain, PDB with high affinity for tau aggregates may be useful as a backbone structure to develop agents for imaging NFTs in AD brains.

Introduction

Alzheimer's disease (AD) is a progressive neurodegenerative disorder characterized by cognitive decline, irreversible memory loss, disorientation, and language impairment. Senile plaques (SPs) composed of β-amyloid (Aβ) peptides and neurofibrillary tangles (NFTs) composed of hyperphosphorylated tau protein in the brain are two pathological hallmarks of AD.[1] Currently, there is no simple and definitive diagnostic method to detect SPs and NFTs in the brain without postmortem pathological staining of brain tissue. Therefore, techniques to image SPs and NFTs *in vivo* are strongly desired.

Recent success in developing several positron emission tomography (PET)/single photon emission computed tomography (SPECT) imaging agents targeting SPs has provided a window of opportunity to improve the diagnosis of AD. Compounds such as [^{11}C]-4-*N*-methylamino-4′-hydroxystilbene (SB-13),[2,3] [^{11}C]-2-(4′-methylaminophenyl)-6-hydroxybenzothiazole (PIB),[4–6] [^{11}C]-2-(2-[2-dimethylaminothiazol-5-yl]ethenyl)-6-(2-[fluoro]ethoxy)benzoxazole (BF-227),[7] [^{11}C]-2-[6-(methylamino)pyridin-3-yl]-1,3-benzothiazol-6-ol (AZD2184),[8] [^{18}F]-2-(1-(2-(*N*-(2-fluoroethyl)-*N*-methylamino)naphthalen-6-yl)ethylidene)malononitrile (FDDNP),[9,10] (*E*)-4-(*N*-methylamino)-4′-(2-(2-(2-[^{18}F]-fluoroethoxy)ethoxy)ethoxy)-stilbene (BAY94-9172),[11,12] (*E*)-4-(2-(6-(2-(2-(2-([^{18}F]-fluoroethoxy)ethoxy)ethoxy)pyridyn-3-ylvinyl)-*N*-methyl benzenamine (AV-45),[13–15] and 2-(3-[^{18}F]-fluoro-4-methylamino-phenyl) benzothiazol-6-ol (GE-067)[16] have been tested clinically and demonstrated potential utility. Although numerous agents targeting SPs have been reported, there are few radiolabeled agents targeting NFTs.

Previous studies have confirmed that NFTs in the hippocampus and entorhinal cortex are positively correlated with the cognitive decline, whereas SPs are found in the brains of both AD patients and cognitively healthy individuals.[17–20] Therefore, NFTs could be a target for imaging by PET/SPECT, enabling a presymptomatic diagnosis and monitoring of the progression and effectiveness of new treatments currently being tested. A previous paper introduced three novel compounds, 4-[2-(2-benzoimidazoyl)ethenyl]-*N*,*N*-diethylbenzenamine (BF-126), 2-[(4-methylamino)phenyl]quinoline (BF-158), and 2-(4-amino-phenyl)quinoline (BF-170), for the *in vivo* imaging of NFTs in the AD brain.[21] Although these probes displayed affinity for NFTs, they also bound to SPs. Since this report, there has been no publication regarding the development of agents to image NFTs despite their clinical significance. Therefore, PET/SPECT probes with greater affinity for NFTs are urgently required.

[a]*Graduate School of Pharmaceutical Sciences, Kyoto University, 46-29 Yoshida Shimoadachi-cho, Sakyo-ku, Kyoto, 606-8501, Japan. E-mail: ono@pharm.kyoto-u.ac.jp; Tel: +81-75-753-4556; Fax: +81-75-753-4568; hsaji@pharm.kyoto-u.ac.jp; +81-75-753-4568; +81-75-753-4608*
[b]*Graduate School of Medicine, Kyoto University, 54 Shogoin-kawaharacho, Sakyo-ku, Kyoto, 606-8507, Japan*
[c]*Department of Neuroscience, Osaka City University Medical School, 1-4-3 Asahi-machi, Abeno-ku, Osaka, 545-8585, Japan*
† Electronic supplementary information (ESI) available. See DOI: 10.1039/c1md00034a

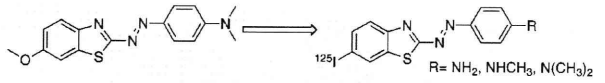

Fig. 1 Chemical structure of ^{125}I-labeled PDB derivatives used in the present study.

Recently, a library containing 72,455 compounds was screened to determine the feasibility of distinguishing tau aggregates from Aβ aggregates with small molecules. Among the compounds which bind to tau aggregates, a phenyldiazenyl benzothiazole (PDB) derivative, 4-[2-(5-methoxy-2-benzothiazolyl)diazenyl]-*N*, *N*-dimethyl-benzenamine (Fig. 1), showed the highest affinity for tau aggregates with two-fold selectivity to bind Aβ aggregates.[22] An even more recent paper reported that the PDB derivative strongly binds to tau aggregates at sites that at least partially overlap with those bound by ThS.[23] These findings prompted us to use the PDB as a core structure in the development of agents to image NFTs. We designed novel radioiodinated PDB derivatives, by substituting a methoxy group with a radioiodine at position 7 and introducing an electron-donating group (dimethylamino, monomethylamino, or amino group) at position 4 of the phenyl group (Fig. 1).

In the present study, we synthesized three radioiodinated PDB derivatives and evaluated their utility for imaging NFTs *in vivo*. To the best of our knowledge, this is the first time PDBs have been proposed as NFT imaging agents for detecting AD.

Results and discussion

The PDB derivatives were prepared as outlined in Scheme 1. We used a diazo coupling reaction to obtain compounds **1**, **2**, and **3**. The tributyltin derivatives (**4**, **5**, and **6**) were prepared from the corresponding compounds (**1**, **2**, and **3**) using a halogen-to-tributyltin exchange reaction catalyzed by Pd(0) in yields of 28.4, 23.7, and 67.3%, respectively. The tributyltin derivatives were used as the starting materials for radioiodination in the preparation of [^{125}I]**7**, [^{125}I]**8**, and [^{125}I]**9**. Novel radioiodinated PDB derivatives were obtained by an iododestannylation reaction using hydrogen peroxide as the oxidant which produced the desired radioiodinated ligands. It was anticipated that the no-carrier-added preparation would result in a final product bearing a theoretical specific activity similar to that of ^{125}I (81.4 TBq mmol^{-1}). The radiochemical identity of the radioiodinated ligands was verified by co-injection with non-radioiodinated compounds from their HPLC profiles. [^{125}I]**7**, [^{125}I]**8**, and [^{125}I]**9** were each obtained in a radiochemical yield of 30–40% with a radiochemical purity of >99% after HPLC.

The affinity of PDB derivatives (**7**, **8**, and **9**) for tau aggregates was evaluated based on inhibition of the binding of thioflavin-S (ThS) to tau aggregates. As shown in Fig. 2A, all derivatives competed well with ThS to bind to tau aggregates, indicating that the binding sites of these compounds in tau aggregates partially overlapped with those of ThS. The K_i values for tau aggregates estimated for **7**, **8**, and **9** were 7.27, 1.37, and 0.48 nM, respectively (Table 1). Several clinical studies found that Aβ imaging agents with K_i values of less than 10 nM successfully detected Aβ plaques in the brain.[24,25] Furthermore, the concentration of tau aggregates (~150 to 300 pmol mg^{-1} of wet tissue) was reported to be higher than that of Aβ aggregates (~9 pmol mg^{-1} of wet tissue) in the frontal and temporal cortices in late-stage AD.[26,27] These findings indicate that **7**, **8**, and **9** have sufficiently high affinity for tau aggregates to image NFTs *in vivo*. Since these compounds inhibited the binding of ThS to tau aggregates, they may have affinity for the β-sheet structure common to both Aβ and tau aggregates. To confirm the selectivity for tau aggregates relative to Aβ aggregates, we evaluated the binding to $Aβ_{1-42}$ aggregates using a competitive assay with ThS. The three derivatives inhibited the binding of ThS to $Aβ_{1-42}$ aggregates and tau aggregates similarly (Fig. 2B). The K_i values for $Aβ_{1-42}$ aggregates estimated for **7**, **8**, and **9** were 6.40, 5.08, and 8.24 nM, respectively (Table 1). The ratio of the K_i values for tau and $Aβ_{1-42}$ aggregates was 0.88 for **7**, 3.71 for **8**, and 17.2 for **9**, indicating the electronegativity of the nitrogen atom of the aminophenyl group to play an important role in determining the selectivity. We also evaluated the affinity of SB-13,[2,3] a well known Aβ imaging probe, for tau and $Aβ_{1-42}$ aggregates according to the same procedure. The K_i values of SB-13 for tau and $Aβ_{1-42}$ aggregates were 82.2 and 81.2 nM, respectively, and the ratio of the K_i value for tau and $Aβ_{1-42}$ aggregates was 0.99. This result indicated that PDB derivatives, especially **9**, have higher selectivity for tau than SB-13. Then, we carried out further binding experiments with AD brain sections using **9**.

Next, [^{125}I]**9** was investigated for its affinity for NFTs by *in vitro* autoradiography in human AD brain sections (Fig. 3). Autoradiographic images of [^{125}I]**9** showed high levels of radioactivity in the brain tissue (Fig. 3A). Furthermore, we confirmed

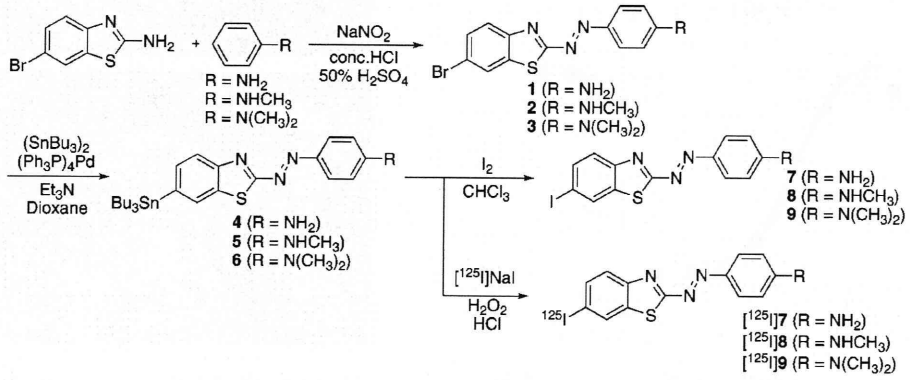

Scheme 1 Synthetic route for PDB derivatives.

Table 1 Inhibition of the binding of thioflavin-S to tau and $A\beta_{1-42}$ aggregates

Compound	K_i/nM[a]		K_i ratios of $A\beta_{1-42}$/tau
	Tau	$A\beta_{1-42}$	
7	7.27 ± 0.09	6.40 ± 0.57	0.88
8	1.37 ± 0.02	5.08 ± 0.45	3.71
9	0.48 ± 0.01	8.24 ± 0.08	17.2
SB-13	82.2 ± 1.91	81.2 ± 1.53	0.99

[a] Values are the mean ± standard error of the mean for three independent experiments.

that the hot spots of [^{125}I]**9** corresponded with those of *in vitro* immunohistochemical staining against phosphorylated tau in sections of the same AD brain (Fig. 3B). Conversely, the normal human brain displayed no remarkable accumulation of [^{125}I]**9** (Fig. 3D). In addition, little radioactivity accumulated in the white matter of the brain (Fig. 3A), indicating that nonspecific signals would be reduced *in vivo*. The hot spots in autoradiography also corresponded with those of *in vitro* immunohistochemical staining against $A\beta_{1-42}$ (Fig. 3C), indicating that PDB derivatives do not have enough selectivity to show high contrast between NFTs and SPs in an autoradiographic study. This result was thought to reflect the higher affinity for both tau and $A\beta_{1-42}$ aggregates of **9** (K_i = 0.48 and 8.24 nM, respectively) than SB-13 (K_i = 82.2 and 81.2 nM, respectively). Therefore, further structural modification of the PDB scaffold is needed to improve the selectivity for tau aggregates.

To further confirm the affinity of **9** for NFTs in the AD brain, fluorescent staining was carried out in sections of brain tissue (Fig. 4). Numerous fluorescent spots were detected in the entorhinal cortex of AD brain sections (Fig. 4A). The fluorescent labeling pattern corresponded to that obtained with ThS

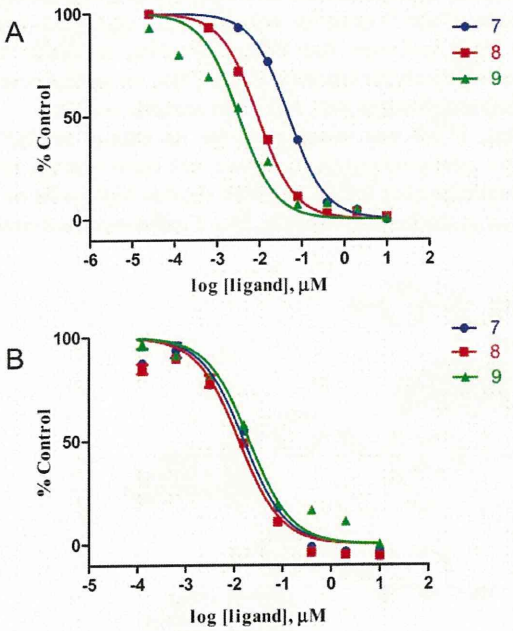

Fig. 2 Inhibition curves for the binding of thioflavin-S to tau (A) and $A\beta_{1-42}$ (B) aggregates.

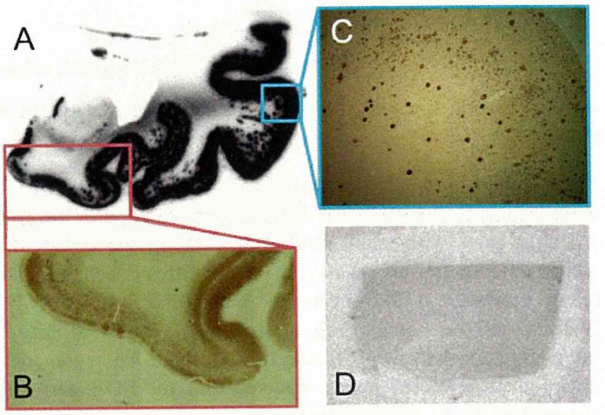

Fig. 3 Autoradiogram of [^{125}I]**9** (A) and immunohistochemical staining with an antibody against phosphorylated tau (B) and $A\beta_{1-42}$ (C) in brain sections from the same patient. Autoradiogram of [^{125}I]**9** in a control brain section (D).

(Fig. 4B). These results, from *in vitro* autoradiography and fluorescent staining, demonstrate the feasibility of using [^{125}I]**9** as a probe for detecting NFTs in the brains of AD patients.

One important requirement for an imaging agent of the brain is to penetrate the blood–brain barrier after an intravenous injection.[28] To evaluate the uptake of PDB derivatives in the brain, biodistribution experiments in normal mice were performed with radioiodinated forms ([^{125}I]**7**, [^{125}I]**8**, and [^{125}I]**9**) (Table 2). The initial uptake of [^{125}I]**7**, [^{125}I]**8**, and [^{125}I]**9** 2 min after the injection was 0.96, 1.03, and 0.94% ID g^{-1}, respectively. The radioactivity then showed a persistent increase, reaching 3.23, 3.13, and 2.89% ID g^{-1}. However, an imaging agent should also be rapidly washed out from the normal brain, in which there is no trapping mechanism for PDB derivatives.[25] Nevertheless, the retention of these probes in the normal mouse brain suggested extensive non-specific binding which would contribute to

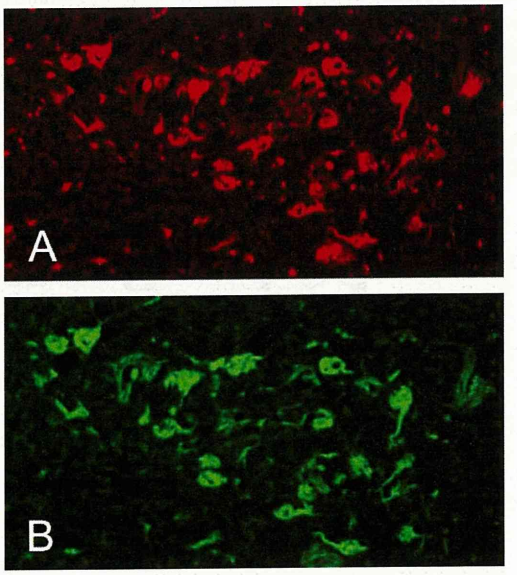

Fig. 4 Fluorescent staining with **9** (A) or thioflavin-S (B) in the entorhinal cortex of an AD brain section.

Table 2 Biodistribution of radioactivity after injection of PDB derivatives in normal mice[a]

Tissue	Time after injection/min			
	2	10	30	60
	[^{125}I]7			
Blood	8.44 (1.10)	4.05 (0.41)	3.27 (0.15)	2.56 (0.26)
Liver	28.5 (2.51)	27.7 (0.51)	19.1 (1.69)	15.5 (1.32)
Kidney	9.54 (0.68)	10.4 (0.75)	9.70 (0.80)	8.88 (0.50)
Intestine	1.18 (0.41)	1.96 (0.60)	7.49 (1.35)	13.6 (3.53)
Spleen	5.78 (1.80)	8.54 (0.43)	8.07 (1.37)	7.84 (1.29)
Pancreas	3.36 (0.37)	5.25 (0.34)	5.22 (0.49)	4.04 (0.40)
Heart	12.8 (1.29)	7.28 (1.53)	5.32 (0.86)	3.58 (0.62)
Lung	18.8 (2.63)	10.0 (0.59)	6.56 (0.27)	5.23 (0.71)
Stomach[b]	0.76 (0.51)	1.28 (0.30)	2.28 (0.16)	3.69 (0.43)
Brain	0.96 (0.07)	1.56 (0.15)	2.50 (0.25)	3.23 (0.39)
	[^{125}I]8			
Blood	6.04 (0.75)	3.64 (0.36)	2.40 (0.31)	1.83 (0.14)
Liver	27.2 (2.66)	23.6 (2.24)	18.6 (2.71)	13.2 (1.36)
Kidney	17.4 (2.68)	17.4 (1.95)	10.8 (1.34)	7.67 (1.37)
Intestine	2.11 (0.41)	6.27 (0.56)	17.1 (0.86)	22.9 (5.47)
Spleen	13.8 (5.09)	17.8 (1.25)	12.2 (1.51)	9.74 (1.26)
Pancreas	4.90 (2.33)	10.7 (2.32)	9.80 (1.64)	7.20 (0.67)
Heart	21.2 (1.28)	12.3 (1.31)	7.2 (2.71)	5.24 (1.36)
Lung	45.7 (4.89)	17.9 (1.56)	8.96 (3.57)	8.96 (1.03)
Stomach[b]	0.81 (0.12)	1.47 (0.20)	2.03 (0.51)	2.28 (0.41)
Brain	1.03 (0.13)	2.02 (0.13)	2.90 (0.23)	3.13 (0.10)
	[^{125}I]9			
Blood	7.12 (1.11)	3.13 (2.20)	2.24 (1.88)	1.55 (1.88)
Liver	25.2 (3.23)	15.2 (4.31)	11.3 (4.85)	6.43 (1.43)
Kidney	11.1 (2.03)	11.3 (1.86)	8.04 (1.44)	9.53 (1.43)
Intestine	1.46 (0.33)	2.80 (0.72)	6.72 (0.76)	8.10 (0.90)
Spleen	5.70 (1.37)	5.92 (1.24)	4.93 (0.75)	3.15 (0.61)
Pancreas	3.04 (0.52)	4.96 (1.12)	5.15 (1.17)	8.11 (1.24)
Heart	12.6 (1.84)	7.15 (2.60)	4.25 (2.52)	4.13 (2.30)
Lung	29.3 (6.05)	11.7(7.63)	7.78 (7.64)	6.55 (8.09)
Stomach[b]	0.71 (0.09)	1.25 (0.11)	2.21 (0.70)	6.34 (6.61)
Brain	0.94 (0.18)	1.56 (0.35)	2.54 (0.40)	2.89 (0.42)

[a] Each value represents the mean (SD) for 5 animals. [b] Expressed as % injected dose per organ.

a high level of background noise *in vivo*. The results suggest that PDB derivatives had unfavorable pharmacokinetics in normal mice, despite their good affinity for tau aggregates. Although factors such as molecular size, ionic charge, and lipophilicity affect a compound's uptake into and washout from the brain, previous studies suggest that lipophilicity is important to improving pharmacokinetics.[2,29,30] Additional structural changes, that is, reducing lipophilicity by introducing a hydrophilic group, are necessary to improve the properties of the PDB derivatives. Improvements to the pharmacokinetics of radioactivity in the brain with high specific binding to tau aggregates should lead to the development of more useful PET/SPECT imaging agents based on the benzothiazole scaffold.

In conclusion, we successfully designed and synthesized three radioiodinated PDB derivatives as probes for the imaging of NFTs in the brain. In binding experiments *in vitro* using tau aggregates, the derivatives, especially **9**, displayed high affinity for tau aggregates. **9** clearly stained NFTs in experiments using autoradiography and fluorescent staining with AD brain sections, reflecting the results of the assays. In biodistribution experiments using normal mice, the PDB derivatives displayed good brain uptake, but persistent radioactivity in the brain made them unsuitable for imaging NFTs *in vivo*. Appropriate structural changes to the PDB scaffold may lead to useful NFT imaging agents.

Acknowledgements

This study was supported by the Funding Program for Next Generation World-Leading Researchers, and a Grant-in-aid for Young Scientists (A) and Exploratory Research from the Ministry of Education, Culture, Sports, Science and Technology, Japan.

References

1 D. J. Selkoe, *Physiol. Rev.*, 2001, **81**, 741.
2 M. Ono, A. Wilson, J. Nobrega, D. Westaway, P. Verhoeff, Z. P. Zhuang, M. P. Kung and H. F. Kung, *Nucl. Med. Biol.*, 2003, **30**, 565.
3 N. P. Verhoeff, A. A. Wilson, S. Takeshita, L. Trop, D. Hussey, K. Singh, H. F. Kung, M. P. Kung and S. Houle, *Am. J. Geriatr. Psychiatr.*, 2004, **12**, 584.
4 C. A. Mathis, Y. Wang, D. P. Holt, G. F. Huang, M. L. Debnath and W. E. Klunk, *J. Med. Chem.*, 2003, **46**, 2740.
5 W. E. Klunk, H. Engler, A. Nordberg, Y. Wang, G. Blomqvist, D. P. Holt, M. Bergstrom, I. Savitcheva, G. F. Huang, S. Estrada, B. Ausen, M. L. Debnath, J. Barletta, J. C. Price, J. Sandell, B. J. Lopresti, A. Wall, P. Koivisto, G. Antoni, C. A. Mathis and B. Langstrom, *Ann. Neurol.*, 2004, **55**, 306.
6 A. Lockhart, J. R. Lamb, T. Osredkar, L. I. Sue, J. N. Joyce, L. Ye, V. Libri, D. Leppert and T. G. Beach, *Brain*, 2007, **130**, 2607.
7 Y. Kudo, N. Okamura, S. Furumoto, M. Tashiro, K. Furukawa, M. Maruyama, M. Itoh, R. Iwata, K. Yanai and H. Arai, *J. Nucl. Med.*, 2007, **48**, 553.
8 A. E. Johnson, F. Jeppsson, J. Sandell, D. Wensbo, J. A. Neelissen, A. Jureus, P. Strom, H. Norman, L. Farde and S. P. Svensson, *J. Neurochem.*, 2009, **108**, 1177.
9 E. D. Agdeppa, V. Kepe, J. Liu, S. Flores-Torres, N. Satyamurthy, A. Petric, G. M. Cole, G. W. Small, S. C. Huang and J. R. Barrio, *J. Neurosci.*, 2001, **21**, RC189.
10 K. Shoghi-Jadid, G. W. Small, E. D. Agdeppa, V. Kepe, L. M. Ercoli, P. Siddarth, S. Read, N. Satyamurthy, A. Petric, S. C. Huang and J. R. Barrio, *Am. J. Geriatr. Psychiatr.*, 2002, **10**, 24.
11 W. Zhang, S. Oya, M. P. Kung, C. Hou, D. L. Maier and H. F. Kung, *Nucl. Med. Biol.*, 2005, **32**, 799.
12 C. C. Rowe, U. Ackerman, W. Browne, R. Mulligan, K. L. Pike, G. O'Keefe, H. Tochon-Danguy, G. Chan, S. U. Berlangieri, G. Jones, K. L. Dickinson-Rowe, H. P. Kung, W. Zhang, M. P. Kung, D. Skovronsky, T. Dyrks, G. Holl, S. Krause, M. Friebe, L. Lehman, S. Lindemann, L. M. Dinkelborg, C. L. Masters and V. L. Villemagne, *Lancet Neurol.*, 2008, **7**, 129.
13 W. Zhang, M. P. Kung, S. Oya, C. Hou and H. F. Kung, *Nucl. Med. Biol.*, 2007, **34**, 89.
14 S. R. Choi, G. Golding, Z. Zhuang, W. Zhang, N. Lim, F. Hefti, T. E. Benedum, M. R. Kilbourn, D. Skovronsky and H. F. Kung, *J. Nucl. Med.*, 2009, **50**, 1887.
15 D. F. Wong, P. B. Rosenberg, Y. Zhou, A. Kumar, V. Raymont, H. T. Ravert, R. F. Dannals, A. Nandi, J. R. Brasic, W. Ye, J. Hilton, C. Lyketsos, H. F. Kung, A. D. Joshi, D. M. Skovronsky and M. J. Pontecorvo, *J. Nucl. Med.*, 2010, **51**, 913.
16 M. Koole, D. M. Lewis, C. Buckley, N. Nelissen, M. Vandenbulcke, D. J. Brooks, R. Vandenberghe and K. Van Laere, *J. Nucl. Med.*, 2009, **50**, 818.
17 P. V. Arriagada, J. H. Growdon, E. T. Hedley-Whyte and B. T. Hyman, *Neurology*, 1992, **42**, 631.
18 H. Braak and E. Braak, *Hippocampus*, 1993, **3**, 239.
19 T. Gomez-Isla, R. Hollister, H. West, S. Mui, J. H. Growdon, R. C. Petersen, J. E. Parisi and B. T. Hyman, *Ann. Neurol.*, 1997, **41**, 17.
20 T. Gomez-Isla, W. Wasco, W. P. Pettingell, S. Gurubhagavatula, S. D. Schmidt, P. D. Jondro, M. McNamara, L. A. Rodes, T. DiBlasi, W. B. Growdon, P. Seubert, D. Schenk, J. H. Growdon, B. T. Hyman and R. E. Tanzi, *Ann. Neurol.*, 1997, **41**, 809.

21 N. Okamura, T. Suemoto, S. Furumoto, M. Suzuki, H. Shimadzu, H. Akatsu, T. Yamamoto, H. Fujiwara, M. Nemoto, M. Maruyama, H. Arai, K. Yanai, T. Sawada and Y. Kudo, *J. Neurosci.*, 2005, **25**, 10857.
22 N. S. Honson, R. L. Johnson, W. Huang, J. Inglese, C. P. Austin and J. Kuret, *Neurobiol. Dis.*, 2007, **28**, 251.
23 N. S. Honson, J. R. Jensen, A. Abraha, G. F. Hall and J. Kuret, *Neurotoxic. Res.*, 2009, **15**, 274.
24 M. P. Kung, C. Hou, Z. P. Zhuang, A. J. Cross, D. L. Maier and H. F. Kung, *Eur. J. Nucl. Med. Mol. Imaging*, 2004, **31**, 1136.
25 H. F. Kung, S. R. Choi, W. Qu, W. Zhang and D. Skovronsky, *J. Med. Chem.*, 2010, **53**, 933.
26 S. Khatoon, I. Grundke-Iqbal and K. Iqbal, *J. Neurochem.*, 1992, **59**, 750.
27 J. Wang, D. W. Dickson, J. Q. Trojanowski and V. M. Lee, *Exp. Neurol.*, 1999, **158**, 328.
28 C. A. Mathis, Y. Wang and W. E. Klunk, *Curr. Pharm. Des.*, 2004, **10**, 1469.
29 M. Ono, H. Kawashima, A. Nonaka, T. Kawai, M. Haratake, H. Mori, M. P. Kung, H. F. Kung, H. Saji and M. Nakayama, *J. Med. Chem.*, 2006, **49**, 2725.
30 Y. Cheng, M. Ono, H. Kimura, S. Kagawa, R. Nishii and H. Saji, *Bioorg. Med. Chem. Lett.*, 2010, **20**, 6141.

Journal of Organometallic Chemistry 696 (2011) 3745–3749

Contents lists available at SciVerse ScienceDirect

Journal of Organometallic Chemistry

journal homepage: www.elsevier.com/locate/jorganchem

Effective synthesis of ^{99m}Tc tricarbonyl complexes by microwave heating

Naoya Harada[a], Hiroyuki Kimura[a,*], Masahiro Ono[a], Daisuke Mori[a], Yoshiro Ohmomo[b], Tetsuya Kajimoto[b], Hidekazu Kawashima[c], Hideo Saji[a,*]

[a] Graduate School of Pharmaceutical Sciences, Kyoto University, 46-29 Yoshida Shimoadachi-cho, Sakyo-ku, Kyoto 606-8501, Japan
[b] Osaka University of Pharmaceutical Sciences, 4-20-1 Nasahara, Takatsuki, Osaka 569-1094, Japan
[c] Kyoto University Hospital, 54 Shogoin Kawahara-cho, Kyoto 606-8507, Japan

ARTICLE INFO

Article history:
Received 16 April 2011
Received in revised form
19 August 2011
Accepted 23 August 2011

Keywords:
^{99m}Tc tricarbonyl complex
Microwave heating
SPECT
Radiopharmaceutical

ABSTRACT

Technetium-99m (^{99m}Tc) is one of the most frequently used nuclides for single-photon emission computed tomography (SPECT) imaging because of its radiochemical characteristics, such as gamma emission of suitable energy (141 keV) and adequate half-life (6.01 h). Although triaquatricarbonyl ^{99m}Tc cation ($[^{99m}Tc(CO)_3(H_2O)_3]^+$) has several advantages as a ^{99m}Tc-labeling agent, e.g., compact chelate size, chelate stability, and simplicity of preparation, its synthetic protocols should be improved. Because microwave heating is a convenient method for synthetic reactions, we studied the effect of microwave irradiation on the synthesis of ^{99m}Tc tricarbonyl complexes. We found several factors beneficial for the preparation of nuclear medicines. In particular, microwave heating promoted one-pot syntheses of ^{99m}Tc tricarbonyl chelates in a short time. In addition, the ^{99m}Tc tricarbonyl complex could be obtained using low concentrations of ligands.

1. Introduction

Single-photon emission computed tomography (SPECT) is a potential tool for applications in nuclear medicine diagnosis, which can permit noninvasive diagnosis of diseases in early stages.

Technetium-99m (^{99m}Tc) is a frequently used nuclide for SPECT imaging because of its radiochemical characteristics such as gamma emission of suitable energy (141 keV) and adequate half-life (6.01 h). We can easily prepare ^{99m}Tc by using a ^{99}Mo–^{99m}Tc generator, which yields Na $^{99m}TcO_4$ as a ^{99m}Tc-containing molecule.

Among several species of ^{99m}Tc, $[^{99m}Tc(CO)_3(H_2O)_3]^+$, which can be prepared using a commercially available kit (IsoLink®) [1], has potential for use as a ^{99m}Tc-labeling agent because it forms compact [2] and stable [3] chelates with tridentate ligands, such as iminodiacetic acid (IDA), picolylamine monoacetic acid (PAMA), and *N,N*-dipicolylamine (DPA). However, for effective synthesis, the reaction of $[^{99m}Tc(CO)_3(H_2O)_3]^+$ with ligands generally requires heating [3–6]. Therefore, we studied improvements in the synthesis of ^{99m}Tc tricarbonyl chelates.

Microwave irradiation provides instantaneous reactions with effective heat conduction and dielectric heating. This method can be clinically used because it is easy and safe to attain reactions at high temperatures [7–9]. One-pot synthesis of ^{99m}Tc-labeled compounds has been previously reported in Ref. [4]. Such methodology is desirable for the synthesis of ^{99m}Tc-labeled compounds because the deprotection step can be avoided under acidic or basic conditions, which may be unsuitable for preparing peptidic probes and antibodies. For these reasons, we designed a novel synthetic protocol of ^{99m}Tc tricarbonyl chelates using microwave reactions. In this paper, we report the development of fast and effective syntheses of ^{99m}Tc tricarbonyl chelates by using microwave heating.

Nitrogen atoms coordinate preferentially to $[Re/^{99m}Tc(CO)_3(H_2O)_3]^+$ compared to oxygen atoms [2]. Although carboxyl groups are not present in DPA, they are contained in IDA and PAMA. Therefore, we hypothesized that IDA, PAMA, and DPA could react differently with $[^{99m}Tc(CO)_3(H_2O)_3]^+$ under microwave irradiation. In addition, these ligands form ^{99m}Tc complexes with various electric charges: IDA forms anionic complexes, PAMA forms neutral complexes, and DPA forms cationic complexes. On the basis of this characteristic, we can synthesize several ^{99m}Tc-labeled probes with various electric charges. For these reasons, we evaluated the effects of microwave irradiation for the synthesis of ^{99m}Tc tricarbonyl complexes by using IDA, PAMA, and DPA.

Abbreviations: DPA, *N,N*-dipicolylamine; IDA, iminodiacetic acid; IDAME, dimethylester of iminodiacetic acid; PAMA, picolylamine monoacetic acid; PAMAEE, ethylester of picolylamine monoacetic acid; RI, radioisotope; SPECT, single-photon emission computed tomography; UV, ultraviolet; HPLC, high-performance liquid chromatography; TLC, thin-layer chromatography.

* Corresponding authors. Tel.: +81 75 753 4566; fax: +81 75 753 4568.
E-mail addresses: hkimura@pharm.kyoto-u.ac.jp (H. Kimura), hsaji@pharm.kyoto-u.ac.jp (H. Saji).

0022-328X/$ – see front matter © 2011 Elsevier B.V. All rights reserved.
doi:10.1016/j.jorganchem.2011.08.033

2. Results and discussion

2.1. Analysis by radio-high performance liquid chromatography

Using an IsoLink kit, $[^{99m}Tc(CO)_3(H_2O)_3]^+$ was obtained in a good radiochemical yield (>95%) (data not shown).

Tc ($Z = 43$) appears in the middle of the second-row transition series in the periodic table of elements and has no stable isotopes. The development of Tc complexes as potential radiopharmaceuticals is facilitated by the use of Re, a group 7 congener of Tc in the periodic table. For this reason, Tc complexes are generally identified by comparison with high-performance liquid chromatography (HPLC) retention time of corresponding Re complexes.

We detected the complexes of Re with various ligands by UV spectra. The benzyl group of **2** was introduced as a chromophore for UV absorption. The HPLC retention times of the Re complexes were 10.9 (**3**), 18.9 (**4**), and 32.4 min (**5**) (Table 1). The HPLC retention times of the ^{99m}Tc complexes were 11.8 (**6**), 19.5 (**7**), and 33.3 min (**8**) (Table 1). Because these RI peaks approximately corresponded to the UV peaks of Re complexes, they can be attributed to the peaks of the ^{99m}Tc complexes.

Table 1
Structures of ^{99m}Tc/Re complexes.

No.	Abbreviation	Structure
3	Bn-IDA–Re	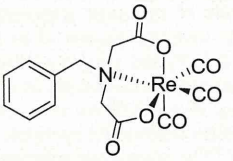
4	PAMA–Re	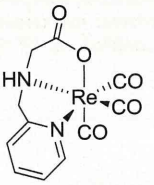
5	DPA–Re	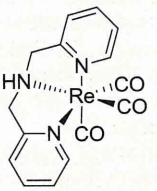
6	Bn-IDA–^{99m}Tc	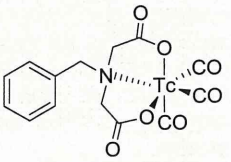
7	PAMA–^{99m}Tc	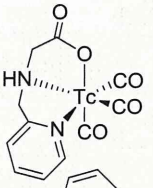
8	DPA–^{99m}Tc	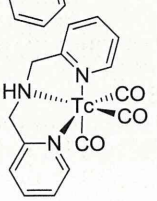

Table 2
HPLC retention time (min) of Re and ^{99m}Tc complexes.

Metal	Bn-IDA[a]–M[d]	PAMA[b]–M[d]	DPA[c]–M[d]
Re	10.9	18.9	32.4
^{99m}Tc	11.8	19.5	33.3

[a] IDA = Iminodiacetic acid.
[b] PAMA = Picolylamine monoacetic acid.
[c] DPA = *N,N*-Dipicolylamine.
[d] M = Metal.

2.2. Determination of reaction temperature

In reactions of 300 μM of Bn-IDAME (dimethylester of iminodiacetic acid) with $[^{99m}Tc(CO)_3(H_2O)_3]^+$ at 75 °C, we could obtain **6** in significantly higher radiochemical yields by using microwave heating than by the conventional method, despite the same reaction temperature (Table 2; Entries 1 and 2). On the basis of these results, it suggested that microwave heating is superior for heat conduction than oil-bath heating.

In reactions at higher temperatures, radiochemical yields increased (Table 2; Entries 2, 3, and 4). This result suggests that $[^{99m}Tc(CO)_3(H_2O)_3]^+$ should be treated with ligands at 110 °C by microwave heating to effectively obtain ^{99m}Tc tricarbonyl complexes.

2.3. Microwave-promoted one-pot synthesis

The effects of microwave heating were observed more clearly in the reactions of $[^{99m}Tc(CO)_3(H_2O)_3]^+$ with Bn-IDAME or PAMAEE (ethylester of picolylamine monoacetic acid) compared to those with *N,N*-dipicolylamine (DPA). The yields of **6** increased more than 50-fold by using microwave heating (Table 3; Entries 1 and 2), and the yields of **7** increased by the same method (Table 3; Entries 3 and 4). Although the yields of **8** increased using microwave heating, the ratio (microwave/oil bath) was only 1.7 (Table 4; Entries 5 and 6). These results suggest that microwave heating promoted the hydrolysis step, which makes this method particularly effective for one-pot syntheses of ^{99m}Tc tricarbonyl complexes.

2.4. Microwave-accelerated synthesis of Bn-IDAME–^{99m}Tc

By the conventional method, the radiochemical yield of the reaction of $[^{99m}Tc(CO)_3(H_2O)_3]^+$ with Bn-IDAME was only 6.4% at 1 min (Table 4). 15–30 min was required to produce **6** in good yields (Table 4). Meanwhile, the radiochemical yield of **6** reached a plateau in just 1 min by microwave heating. These results show that microwave heating enabled rapid production of ^{99m}Tc tricarbonyl complexes. Rapid synthesis is essential in nuclear medicine because it can suppress the decrease of radioactivity and

Table 3
Effect of temperature on the synthesis of Bn-IDA–^{99m}Tc.

Entry	Ligand	[Ligand] (μM)	Method	Temp. (°C)	Time (min)	Yield (%)
1	Bn-IDAME	300	Oil bath	75	30	29.7
2	Bn-IDAME	300	Microwave[a]	75	30	51.5
3	Bn-IDAME	300	Microwave[a]	90	30	86.9
4	Bn-IDAME	300	Microwave[a]	110	30	98.5

[a] Heated with microwave radiation (300 W, 17 bar maximum pressure).

Table 4
Ratios of radiochemical yields of ^{99m}Tc complexes by microwave heating to that by oil-bath heating.

Entry	Ligand	Product	[Ligand] (μM)	Method	Temp. (°C)	Time (min]	Yield (%)	Yield ratio (Microwave/oil bath)
1	Bn-IDAME	**3**	300	Microwave[a]	110	30	78.6	52.4
2	Bn-IDAME	**3**	300	Oil bath	75	30	1.5	
3	PAMAEE	**4**	30	Microwave[a]	110	5	93.4	11.7
4	PAMAEE	**4**	30	Oil bath	75	5	8.0	
5	DPA	**5**	30	Microwave[a]	110	5	84.9	1.7
6	DPA	**5**	30	Oil bath	75	5	49.0	

[a] Heated by microwave radiation (300 W, maximum pressure was 17 bar).

avoiding long-time heating of precursors, particularly those of peptides and antibodies.

2.5. Decrease in concentrations of ligands by microwave heating

Although **6** could be obtained in more than 90% radiochemical yield by the conventional method, a high concentration of Bn-IDAME (30 mM) must be employed (Table 5). Moreover, the radiochemical yield of **6** was high (>90%) only when the concentration of Bn-IDAME was higher than 30 μM.

In contrast, by microwave heating, the radiochemical yield of **6** was high (>90%), although the concentration of Bn-IDAME was 30 μM. Moreover, we could obtain **6** by microwave heating with only 30 nM of Bn-IDAME (Table 6).

These results imply that concentrations of precursors can be decreased using microwave heating. Therefore, this method is considered to be beneficial for the preparation of probes. It is usually impossible to separate labeling precursors and ^{99m}Tc-labeled compounds. Free precursors may not only inhibit the binding of ^{99m}Tc-labeled compounds to target molecules but also cause adverse effects [11]. Such issues can be avoided by microwave heating.

3. Conclusion

We were able to more effectively synthesize ^{99m}Tc tricarbonyl complexes by microwave heating than by the conventional method. We rapidly obtained ^{99m}Tc tricarbonyl complexes by microwave heating using lower concentrations of ligands than that required by the conventional method. In addition, we demonstrated that microwave heating can be employed for ^{99m}Tc tricarbonyl complex synthesis. Hence, microwave heating can be efficiently used in nuclear medicine.

4. Material and methods

4.1. General procedure

Kieselgel 60 F-254 plates (Merck, Germany) were used for thin-layer chromatography (TLC). W-Prep 2XY (Yamazen, Japan) was used for silica gel column chromatography. Hi Flash™ silica gel column 40 mm 60 Å (Yamazen) was used as the column. LC-20AD (Shimadzu, Japan) was used for HPLC. SPD-20A (Shimadzu) and NDW-351D (Aloka, Japan) were employed as ultraviolet (UV; $\lambda = 254$ nm) and radioisotope (RI) detectors, respectively. Cosmosil 5C18-AR-II 10 mm × 250 mm (Nacalai Tesque, Japan) was used as the HPLC column. Methanol (0.1% trifluoroacetic acid) and nanopure water (0.1% trifluoroacetic acid) were used as the mobile phase (flow rate = 2 mL/min). Nanopure water was prepared by MQ Integra15 (Nihon Millipore, Japan). ^{1}H and ^{13}C NMR spectra were recorded on LNM-AL500 (JEOL, Japan) with $CDCl_3$, DMSO-d_6, or CD_3OD as a solvent and with tetramethylsilane as an internal standard (Euriso-Top, France). Mass spectra were recorded on LCMS-2010 EV (Shimadzu) or JMS-SX 102A QQ (JEOL). Discover (CEM Japan, Japan) was used as the microwave reactor. The maximum energy of microwave irradiation was set at 300 W, and the maximum pressure was set at 17 bar. All chemicals used were of reagent grade.

4.2. Selection of tridentate ligands

We selected three tridentate ligands that have amino groups, carboxyl groups, or pyridyl groups as the coordinating groups. To avoid hindrance in the synthesis of precursors, we protected free carboxyl groups as esters in this study.

4.3. Chemistry

4.3.1. Triaquatricarbonylrhenium bromide (*1*)

1 was prepared as previously reported in Ref. [10]. Briefly, 5 g of $Re(CO)_5Br$ (Strem Chemicals, USA) was suspended in excess water and refluxed for 1 day. The reaction mixture was lyophilized to yield **1** as a chamois solid (4.4 g; 89% yield).

4.3.2. Dimethyl 2,2′-(benzylanedily)diacetate (Bn-IDAME) (*2*)

To a solution of dimethyl iminodiacetate (2.4 g; Fluka, USA) in 5 mL of anhydrous dimethylformamide, benzyl bromide (2.1 g; Aldrich, USA) and K_2CO_3 (2.1 g; Nacalai Tesque) were added. The mixture was stirred at 60 °C for 14 h and extracted with diethyl ether. The organic phase was washed with brine and dried with Na_2SO_4 (Nacalai Tesque). Purification by silica gel chromatography (hexane/AcOEt = 2/1) yielded **2** as a pale yellow oil (2.8 g; 87% yield). TLC Rf = 0.42 (hexane/AcOEt = 2/1). ^{1}H NMR (500 MHz,

Table 5
Difference in reaction kinetics between microwave heating and oil bath for synthesis of **6**.

Method	Time (min)						
	1	5	10	15	30	60	
Microwave[a]	93.1	90.7	90.7	91.2	93.6	92.0	Yield (%)
Oil bath[b]	6.4	51.7	71.5	83.6	88.9	89.5	

[a] Heated by microwave radiation (300 W, 17 bar maximum pressure) at 110 °C, [Bn-IDAME] was 30 mM.
[b] Heated by oil bath at 75 °C, [Bn-IDAME] was 30 mM.

Table 6
Effect of microwave heating on concentration of ligands for synthesis of **6**.

Method	[Ligand] (M)						
	3×10^{-2}	3×10^{-3}	3×10^{-4}	3×10^{-5}	3×10^{-6}	3×10^{-7}	
Microwave[a]	96.6	98.5	97.9	78.6	47.2	30.9	Yield (%)
Oil bath[b]	91.9	87.3	33.8	1.5	0.0	0.0	

[a] Heated by microwave radiation (300W, 17 bar maximum pressure) at 110 °C for 30 min.
[b] Heated by oil bath at 75 °C for 30 min.

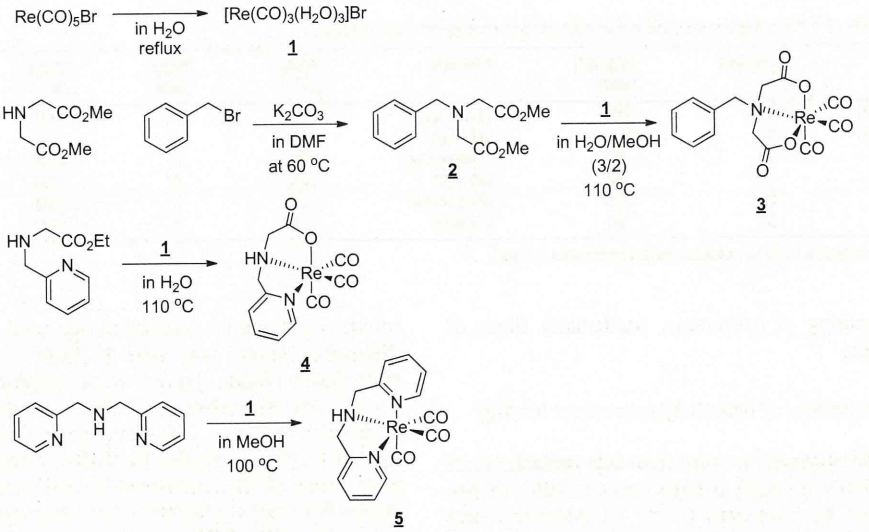

Scheme 1. Synthesis of rhenium tricarbonyl complexes.

CD_3OD) $\delta = 7.35$ (d, $J = 7.4$ Hz, 2H), 7.30 (dd, $J = 7.4$, 6.9 Hz, 2H), 7.25 (d, $J = 6.9$ Hz, 1H), 3.87 (s, 2H), 3.70 (s, 6H), 3.51 (s, 4H). ^{13}C NMR (125 MHz, $CDCl_3$) $\delta = 51.4$, 54.0, 58.0, 127.4, 128.4, 129.0, 138.2, 171.5. FAB–HRMS; 252.1230 $[M + H]^+$ for $C_{13}H_{18}NO_4$ calcd 252.1236.

*4.3.3. Bn-IDA–Re (**3**) [Re(CO)$_3${NH(CH$_2$COO)$_2$}]H*

To a solution of **2** (0.70 g) in 1,4-dioxane/water (6 mL/4 mL), NaOH (0.29 g) was added. The mixture was stirred at 60 °C for 0.4 h. To the mixture was added 6 N HCl to adjust the pH to 7. The solvent was removed under reduced pressure. The crude sample was added in a microwave vial and dissolved in 10 mL of water. To the vial was added **1** (0.40 g). The reaction vial was crimp sealed prior to microwave heating at 110 °C for 5 min. The reaction mixture was chilled, and then the precipitate was filtered and washed with ice-cold water to yield **3** (0.11 mg; 22%). ^1H NMR (500 MHz, DMSO-d_6) $\delta = 7.64$ (m, 2H), 7.40 (m, 3H), 4.33 (s, 2H), 3.88 (d, $J = 14.89$ Hz, 2H), 2.74 (d, $J = 14.89$ Hz, 2H). ESI-MS; 492 $[M]^-$ for $C_{14}H_{11}NO_7Re$.

*4.3.4. PAMA–Re (**4**)*

1 (0.20 g) and 0.10 g of PAMAEE (Tokyo Chemical Industry, Japan) were added to a microwave vial and dissolved in water/methanol (3 mL/0.5 mL). The reaction vial was crimp sealed prior to microwave heating at 110 °C for 5 min. The reaction mixture was chilled, and the precipitate was collected by filtration and washed with dichloromethane to yield **4** (white powder; 0.13 g; 56% yield). ^1H NMR (500 MHz, DMSO-d_6) $\delta = 8.81$ (d, $J = 5.5$ Hz, 1H), 8.12 (dt, $J = 7.8$, 1.1 Hz, 1H), 7.75 (d, $J = 7.8$ Hz, 1H), 7.57 (t, $J = 6.6$ Hz, 1H), 7.22 (t, $J = 6.2$ Hz, 1H), 4.58 (d, $J = 16.7$ Hz, 1H), 4.50 (dd, $J = 5.1$, 16.6 Hz, 1H), 3.65 (dd, $J = 8.1$, 17.3 Hz, 1H), 3.25 (d, $J = 17.3$ Hz, 1H). ^{13}C NMR (125 MHz, DMSO-d_6) $\delta = 53.9$, 62.0, 123.7, 125.4, 140.2, 152.0, 160.0, 179.5, 197.4, 197.5, 197.8. FAB–HRMS; 437.0148 $[M + H]^+$ for $C_{11}H_{10}N_2O_5Re$ calcd 437.0131.

*4.3.5. DPA–Re (**5**) [Re(CO)$_3${NH(CH$_2$C$_5$H$_4$N)$_2$}]Br*

1 (75 mg) and 0.37 g of DPA (Tokyo Chemical Industry) were added to a microwave vial and dissolved with 1 mL of methanol. The reaction vial was crimp sealed prior to microwave heating at 100 °C for 5 min. **5** was recrystallized from ethyl acetate/hexane (yellow solid; 69 mg; 77% yield). ^1H NMR (500 MHz, DMSO-d_6) $\delta = 8.86$ (d, $J = 5.4$ Hz, 2H), 8.00 (dt, $J = 7.7$, 1.4 Hz, 2H), 7.62 (d, $J = 7.7$ Hz, 2H), 7.42 (t, $J = 6.6$ Hz, 2H), 4.79 (dd, $J = 17.5$, 6.0 Hz, 2H), 4.74 (d, $J = 17.2$ Hz, 2H). ^{13}C NMR (125 MHz, $CDCl_3$) $\delta = 61.7$, 123.3, 125.4, 140.2, 151.7, 161.0, 196.0, 196.1. FAB–HRMS; found: 470.0515 $[M]^+$ for $C_{15}H_{13}N_3O_3Re$ calcd 470.0498.

*4.3.6. Bn-IDA–^{99m}Tc (**6**)*

In the present study, we used $[^{99m}Tc(CO)_3(H_2O)_3]^+$ prepared as previously reported in Ref. [1]. Briefly, Na $^{99m}TcO_4$ (Technescinti-10M®, Nihon Medi-Physics, Japan) was added into an IsoLink® kit (Mallinckrodt, Netherlands), and the kit was heated at 100 °C for 20 min (247 MBq/mL). First, 240 μL of water and 80 μL of $[^{99m}Tc(CO)_3(H_2O)_3]^+$ were added to 240 μL of a methanol solution of **2** (70 mM, 7.0 mM, 0.70 mM, 70 μM, 7.0 μM, or 0.70 μM). Next, 6 M hydrochloric acid was added to the mixture to adjust the pH to 8. The mixture was heated on a microwave reactor or in an oil bath. HPLC t_R; 11.8 min (methanol/water = 80/20).

*4.3.7. PAMA–^{99m}Tc (**7**)*

First, 240 μL of water and 80 μL of $[^{99m}Tc(CO)_3(H_2O)_3]^+$ were added to 240 μL of methanol solution of PAMAEE (0.70 mM or 70 μM). Next, 6 M hydrochloric acid was added to the mixture to adjust the pH to 8. The mixture was heated in a microwave reactor or in an oil bath. HPLC t_R; 19.5 min (methanol/water = from 40/60 to 60/40 over 30 min).

*4.3.8. DPA–^{99m}Tc (**8**)*

First, 40 μL of water and 160 μL of $[^{99m}Tc(CO)_3(H_2O)_3]^+$ were added to 800 μL of a methanol solution of DPA (37.5 μM or 3.75 μM). Next, 6 M hydrochloric acid was added to the mixture to adjust the pH to 8. The mixture was heated on a microwave reactor or in an oil bath. HPLC t_R; 33.3 min (methanol/water = from 30/70 to 40/60 over 20 min and then from 40/60 to 80/20 over 20 min) (Scheme 1).

4.4. Analysis by radio-HPLC

Radiochemical yields were calculated from the RI peak area of the HPLC chart. After reactions, the reaction samples were purified by HPLC. Then, radioactivity was dynamically plotted to obtain the RI chart. We calculated (radioactivity of objective compound)/(total radioactivity) as yield of ^{99m}Tc complexes.